Dalton Transactions

Accepted Manuscript

ROYAL SOCIETY OF CHEMISTRY

www.rsc.org/dalton

Asymmetric Oxidation of Bridging Vinyl- and Ethynyl Terthiophene Ligands in Trinuclear Ruthenium Complexes

Jing Zhang,[a] Chao-Fang Sun,[a] Ming-Xing Zhang,[a] František Hartl,*[,b] Jun Yin,[a] Guang-Ao Yu,[a] Li Rao,[a] Sheng Hua Liu*[,a]

[a]*Key Laboratory of Pesticide and Chemical Biology, Ministry of Education, College of Chemistry, Central China Normal University, Wuhan 430079, P.R. China*

[b]*Department of Chemistry, University of Reading, Whiteknights, Reading RG6 6AD, U.K.*

Abstract

A series of ruthenium(II) complexes $[\{RuCl(CO)(PMe_3)_3(-CH{=}CH-)\}_nX]$, **1a−1c** (**1a**: n = 3, X = 3,3"-dimethyl-2,2':3',2"-terthiophene; **1b**: n = 2, X = 2,2'-bithiophene; **1c**: n = 2, X = 2,3-bis(3-methylthiophen-2-yl)benzothiophene) and $[\{Cp^*(dppe)_2Ru(-C{\equiv}C-)\}_3X]$, **1d** (X= 3,3"-dimethyl-2,2':3',2"-terthiophene), were prepared and characterized by ^1H, ^{13}C and ^{31}P NMR. Their redox, spectroscopic and bonding properties were studied with a range of spectro-electrochemical methods in combination with density functional theory calculations. The first two anodic steps observed for **1a** and **1d** are largely localized on the lateral frameworks of the molecular triangle, the direct conjugation between them being precluded due to the photostable open form of the dithienyl ethene moiety. The third anodic step is then mainly localized on the centerpiece of the triangular structure, affecting both bithiophene laterals. The experimental IR and UV-vis-NIR spectroelectrochemical data and, largely, also DFT calculations account for this explanation, being further supported by direct comparison with the anodic behavior of reference diruthenium complexes **1b** and **1c**.

Keywords: Ruthenium Complex; Spectroelectrochemistry; DFT Calculations; Oligothiophene Bridge; Localized Oxidation; Molecular Wire.

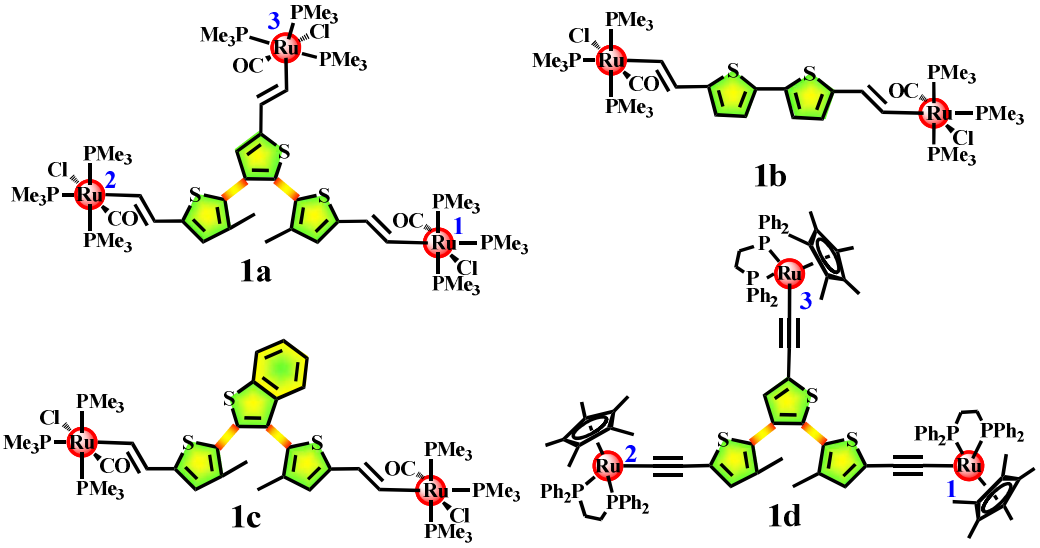

Chart 1. The studied series of oligonuclear ruthenium complexes **1a-1d** bridged by vinyl- and ethynyl oligothiophene ligands.

Introduction

Studies of bridge-mediated electron transfer between terminal organic, organometallic and inorganic probes have been spurred by the interest in fundamentals of directional electron transfer and prospects in building highly functionalized molecules essential for implementation of molecular electronic devices.[1-3] In this regard, thorough understanding and accurate control of the nature and strength of interactions between the redox active molecular components are of particular importance. Compounds with redox-active organometallic termini, herein represented by oligonuclear ruthenium complexes linked by conjugated organic ligands, belong to the most promising systems for applications as molecular wires due to their easy functionalization and controllability, and low costs of the implemented organic molecules.[4-7]

In recent years, oligothiophenes, and even dithienylethene (DTE) derivatives, as bridging ligands have been introduced to organometallic systems, with an accent on their versatile electrochemical and photochemical properties.[8-11] Wenger and co-workers focused on the α,α'-bis(diphenylamino)-substituted bithiophene

derivative[12], while the groups of Chen and Liu jointly explored two different types of dinuclear ruthenium alkynyl complexes connected by the bithiophene bridge[13]. These complexes feature remarkable propensity for electronic delocalization and exhibit a promising potential for implantation in nanoscopic molecular devices. Studies devoted to mixed-valence systems with symmetrical and delocalized organic structures commonly include two identical redox-active centers. Reports on mixed-valence systems with more than two identical or closely related redox centers are scarce.[14-17] Furthermore, most of the reported trimetallic complexes are of C_3-symmetry interlocked triskelion shape with a single ring bridge and examples of their partially localized oxidation are rare.[16a, 16b, 16c] Therefore, we have designed and synthesized triangular triruthenium complex **1a** (Chart 1) with a more complicated non-C_3-symmetric terthiophene bridge based on a combination of two reference divinyl bithiophene-bridged diruthenium complexes **1b** sharing one of the Ru centers and containing the open dithienyl ethene structural motif (Chart 1). The triple-redox-site system of **1a** was envisaged to provide a dual path for directional electron transfer between the central and lateral ruthenium centers through each of the bithiophene linkers. In order to gain deeper insight into the electronic properties of oxidized **1a**, we have also synthesized another reference diruthenium complex **1c** (Chart 1) featuring only the "disconnected" dithienyl ethene bridge. Furthermore, we have added a new ethynyl thiophene-bridged triruthenium complex (**1d**) similar to **1a**. The replacement of the vinyl moiety aimed at tracking the oxidation evolution of the bridging ligand with the aid of the key signaling data from the spectator C≡C bond (Chart 1) and further deciphering the intriguing anodic behavior of the terthiophene core in **1a** decorated by the distant carbonyl spectator ligands. Our original intention was to investigate the electronic coupling in the open-triangle systems **1a** and **1d** as well as their photocyclized (closed) forms[18]. Unfortunately, both triruthenium complexes were found to be photostable upon irradiation with UV light. On the other hand, the photostability facilitated the spectro-electrochemical studies. The oxidation processes and the related electron transfer properties of triangular complexes **1a** and **1d** and reference dinuclear systems **1b** and **1c** were investigated by

controlled-potential voltammetry, UV-vis-NIR-IR spectroelectrochemistry and density functional theory calculations.

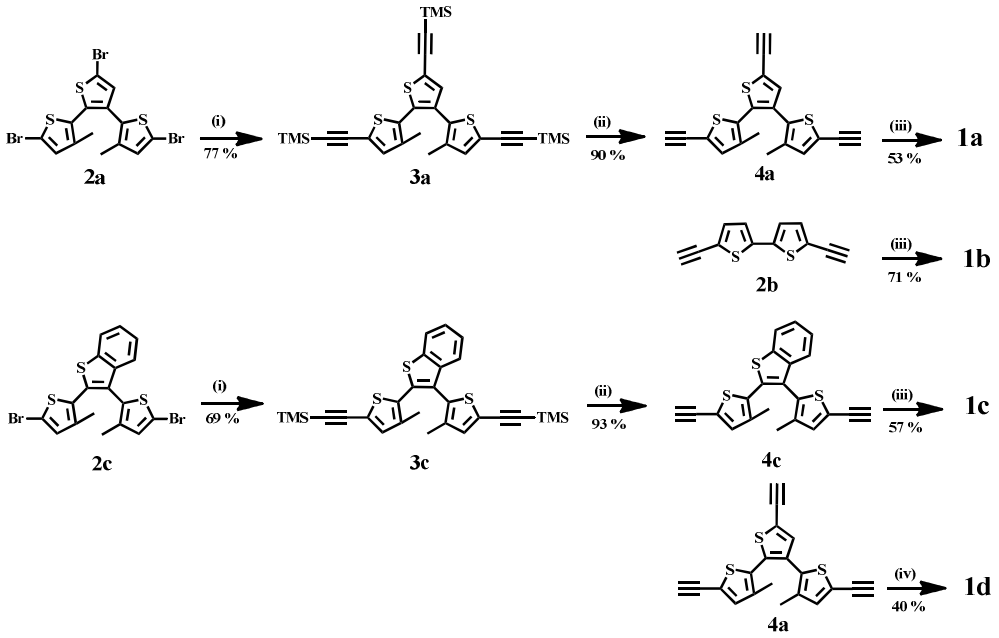

Scheme 1. General synthetic routes to complexes **1a-1d**. Reagents and conditions: (i) $[Pd(PPh_3)_4]$, CuI, Et_3N, trimethylsilylacetylene in toluene; (ii) KOH, THF/MeOH; (iii) $[RuHCl(CO)(PPh_3)_3]$, PMe_3, in CH_2Cl_2; (iv) $[RuCl(\eta^5\text{-}C_5Me_5)(dppe)]$, $Na[BPh_4]$, DBU (1,8-diazabicyclo[5.4.0]undec-7-ene), Et_3N, in THF.

Results and Discussion

Syntheses and Characterization

The 3,3''-dimethyl-2,2':3',2''-terthiophene unit was prepared according to the synthetic route presented in Scheme 1, using a modified literature method[18a]. The trimethylsilyl-protected precursors **3a** and **3c** were synthesized by the $[Pd(PPh_3)_4]$ / CuI-catalyzed Sonogashira cross-coupling reaction between **2a**, **2c** and trimethylsilylacetylene, respectively. The ligand precursors were smoothly converted into corresponding ethynyls **4a** and **4c** by the removal of the protecting trimethylsilyl groups with dilute aqueous KOH in MeOH–THF. The diethynyl oligothiophenes (**2b** and **4c**) and triethynyl terthiophene (**4a**) were then reacted with $[RuHCl(CO)(PPh_3)_3]$

to give the penultimate insertion products. The latter five-coordinate complexes were not isolated because of their air-sensitivity, especially in solution. Instead, PMe_3 was added directly to give ultimate six-coordinate products **1a**-**1c**. Finally, triethynyl terthiophene (**4a**) was reacted directly with [RuCl(η^5-C_5Me_5)(dppe)] to obtain product **1d**.

Photostability was encountered for the whole series of studied dithienyl ethene complexes, including target complexes **1a**, **1c** and **1d** and their precursors **2a**-**4a** and **2c**-**4c**. No photocyclization of the complexes to the colored closed forms absorbing lower-energy photons was observed during irradiation of the THF and CH_2Cl_2 solutions in quartz cuvettes with 302-nm or 365-nm light for more than 30 min, in some cases even several hours.

Complexes **1a**-**1d** have been characterized by ^{1}H, ^{13}C, and ^{31}P NMR. Despite of the distinct bridging ligands in complexes **1a**-**1c**, the resonance signals of the vinyl protons in the ^{1}H NMR spectra, Ru–C≡O in the ^{13}C NMR spectra and PMe_3 in the ^{31}P NMR spectra exhibit no significant differences. Notably, there are two different carbonyl signals (at δ 202.20 and 207.11) in the ^{13}C NMR spectrum of **1a**, reflecting that the Ru1 and Ru2 centers are electronically slightly different from Ru3 (Chart 1).

Electrochemical Studies

Cyclic voltammetry (CV) and square-wave voltammetry (SWV) were used to study the redox behavior of complexes **1a**-**1d** in a low-polarity solvent (CH_2Cl_2) containing either a common supporting electrolyte, *n*-Bu_4NPF_6, or a weakly coordinating electrolyte, *n*-$Bu_4N[B(C_6F_5)_4]$. Reference CV plots recorded for the corresponding TMS-terminated bridging ligands **3a** and **3c** show no redox waves in the potential interval -1.0 to +1.0 V (Figure S1). Cyclic and square-wave voltammograms recorded for complexes **1a**-**1c** and **1d** are depicted in Figures 1 and S2 (Supplementary Information), and the corresponding anodic potential data are presented in Table 1. Diruthenium complexes **1b** and **1c** undergo two successive one-electron oxidations corresponding to pairs of well-separated reversible anodic waves. Probing oxidation of triruthenium complexes **1a** and **1d**, two anodic reversible

waves are followed by a third one that is electrochemically quasi-reversible in both cases (Figures 1 and S2). Owing to ion-paring effects, the anodic wave separation ($\Delta E_{1/2}$) for complexes **1a**-**1d** is smaller in the *n*-Bu_4NPF_6 electrolyte than in the *n*-$Bu_4N[B(C_6F_5)_4]$ electrolyte[19-22]. In addition, the $E_{1/2}$ (1) value of **1c** is much larger than those of **1a** and **1b**, which may be caused by additional involvement of the phenyl ring stabilizing the HOMO.

The following analysis has focused on the three successive one-electron oxidation processes of **1a**. For convenience, the three metal centers in **1a** and **1d** have been denoted as Ru1 (right), Ru2 (left) and Ru3 (middle) (Chart 1). Compared with **1b** and **1c**, the electrode potential values for the first and second oxidation of complex **1a** are close to those of complex **1b**. Thus, we have assumed that the first two anodic steps observed for **1a** are largely on the lateral framework (the Ru1 or Ru2 vinyl thiophene moieties). The direct conjugation is broken between the Ru1 and Ru2 centers for the open form of the dithienyl ethene unit. The third anodic step is then mainly on the central part of the open triangle, i.e., the Ru3 vinyl thiophene moiety. At this point it is also worth mentioning that the bridging ligand significantly participates in the oxidation of **1a** according to DFT calculations presented below. The electrochemical data recorded for **1d** also provide a reasonable evidence for the above assumption, for the electrode potentials of the first two anodic steps are again fairly close, implying that the oxidations occur at Ru1 or Ru2 ethynyl thiophene sites. Their stepwise appearance instead of an unresolved two-electron anodic wave is indicative of a non-zero electronic coupling between the ruthenium termini mediated by the conjugated V-shaped terthiophene center. The oxidation potential for the third anodic step of **1a** and **1d** is indeed much higher, implying involvement of the central part of the bridge. The following spectroelectrochemical sections present strong evidence for this assignment based on the analysis of the CV data.

Table 1. Electrochemical data for complexes **1a-1d**[a]

Complex	$[X]^-$	$E_{1/2}(1)$ (V)	$E_{1/2}(2)$ (V)	$E_{1/2}(3)$ (V)
1a	$[PF_6]^-$	0.080	0.308	0.680
	$[B(C_6F_5)_4]^-$	0.100	0.344	0.700
1b	$[PF_6]^-$	0.105	0.348	--
	$[B(C_6F_5)_4]^-$	0.125	0.405	--
1c	$[PF_6]^-$	0.335	0.505	--
	$[B(C_6F_5)_4]^-$	0.294	0.495	--
1d	$[PF_6]^-$	−0.244	−0.157	0.112
	$[B(C_6F_5)_4]^-$	−0.275	−0.159	0.114

[a] Electrode potentials in CH_2Cl_2 containing 1 mM **1a-1d** and 10^{-1} M *n*-Bu_4NPF_6 or 5×10^{-2} M *n*-$Bu_4N[B(C_6F_5)_4]$. An Ag/Ag^+ reference electrode (internal solution 10^{-2} M $AgNO_3$ + 10^{-1} M *n*-$Bu_4N[X]$ in acetonitrile) was used. The $E_{1/2}$ value for the ferrocene/ferrocenium (Fc/Fc^+) couple was found at +0.23 V under these conditions.

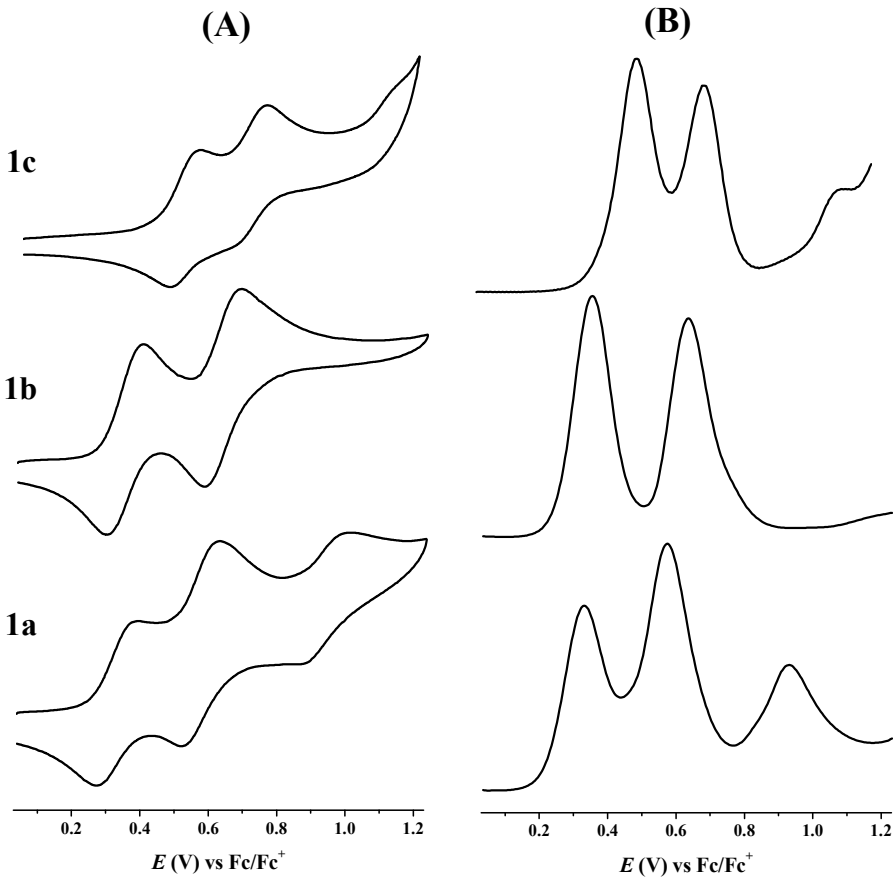

Figure 1. (A) Cyclic voltammograms (CV) of complexes **1a-1c** in CH_2Cl_2/*n*-$Bu_4N[B(C_6F_5)_4]$ at 100 mV s^{-1} and (B) corresponding square-wave voltammograms (SWV) at f = 10 Hz (t_p = 25 mV).

UV-vis-NIR Spectroelectrochemical Studies

In order to obtain insight into the oxidation processes of **1a-1d**, *in situ* spectroelectrochemical studies were carried out at the separate anodic waves presented in Table 2. Spectral changes in the UV-vis-NIR region are shown in Figures 2 (**1a**) and S3-S5 (**1b-1d**). The corresponding absorption maxima and molar absorptivities are listed in Table 2.

The electronic absorption spectra of neutral complexes **1a-1d** are dominated by intense bands in the near-UV to 22000 cm^{-1} (450 nm) region, originating largely from intraligand transitions mixed with some MLCT contribution[23]. Upon the stepwise oxidation of neutral reference **1b** to $[\mathbf{1b}]^{+}$, the amplitude of the strong absorption band at 24038 cm^{-1} (416 nm) gradually decreased and strong absorptions appeared simultaneously in the NIR region and around 14300 cm^{-1} (700 nm) (Figure S3, top). Further oxidation to stable $[\mathbf{1b}]^{2+}$ led to complete disappearance of the absorption bands between 20000 cm^{-1} (500 nm) and 6667 cm^{-1} (1500 nm) and a broadened absorption remained at 22989 cm^{-1} (435 nm) (Figure S3, bottom).

In contrast to the oxidation of **1b**, only very weak NIR absorption at ca 10500 cm^{-1} and small changes in absorption around 16667 cm^{-1} (600 nm) could be observed in the course of the oxidation of **1c** to the corresponding mono- and dications. The intense absorption in the UV region varied only marginally (Figure S4). The inherent stability of $[\mathbf{1c}]^{+}$ and $[\mathbf{1c}]^{2+}$ has been confirmed separately by chemical doping combined with cyclic voltammetry (see below).

Monitoring the electrochemical oxidation of triruthenium complex **1a** in the three consecutive steps has revealed a more complex behavior compared to diruthenium reference **1b**. Oxidation of neutral **1a** to $[\mathbf{1a}]^{+}$ results in simultaneous appearance of new intense absorption in the near-IR region and a structured band at 14620 cm^{-1} (684 nm) (Figure 2, top), similar to the low-energy absorption of $[\mathbf{1b}]^{+}$. Importantly, the subsequent oxidation to $[\mathbf{1a}]^{2+}$ at the second anodic wave promoted further growth of the characteristic visible-NIR absorption that reached its maximum intensity (Figure 2, middle). Finally, the third anodic step producing $[\mathbf{1a}]^{3+}$ led to

complete disappearance of the NIR absorption and strongly diminished the 684-nm absorption, with a slightly broader absorption at 14410 cm^{-1} (694 nm) left behind (Figure 2, bottom). The latter process strongly resembles the oxidation of reference $[\mathbf{1b}]^{+}$ to $[\mathbf{1b}]^{2+}$.

With regard to the oxidative evolution of the triethynyl triruthenium complex, **1d**, the UV-vis-NIR spectral changes accompanying the first two consecutive anodic steps (Figure S5, top and middle) were almost identical to those recorded for complex **1a**. Remarkably, in the course of the third anodic step converting $[\mathbf{1d}]^{2+}$ to $[\mathbf{1d}]^{3+}$ a new strong NIR absorption band arose at 10471 cm^{-1} in parallel with the decay of the two original NIR absorption bands. The closely related trivinyl triruthenium complex, $[\mathbf{1a}]^{3+}$, does not feature such a strong NIR absorption (Figure 2, bottom). We assume that the first two oxidations of **1a** and **1d** are similar, residing on the lateral vinyl- and ethynyl-dithiophene units, while the third one involves a different central part of the complexes, that is, vinyl vs. ethynyl linkers or even the different ancillary ligands. This is also indicated by changes in the ν(CO) and ν(C≡C) stretching wavenumbers revealed below by IR spectroelectrochemistry. To further refine on the description of the redox series based on the spectroelectrochemical experiments, the UV-vis-NIR spectral changes induced by the stepwise oxidation of complex **1a** were also recorded for the corresponding cation, dication and trication formed by oxidation with added equivalent amounts of thianthrenium hexafluorophosphate ($TAPF_6$) (Figure S6). All three anodic potentials of **1a** (Table 1) are less positive than that of the oxidation of thianthrene (TA) to its radical cation ($E_{1/2}$ = +0.82 V *vs*. Fc/Fc^{+})[24, 25]. When **1a** in dichloromethane was gradually treated with 0 to 1 equiv. of $TAPF_6$ and then with additional 1 equiv., the intense absorption in the near-UV region was decreasing gradually and several overlapping bands emerged between 16667 cm^{-1} (600 nm) and 6667 cm^{-1} (1500 nm). As expected, the intensity of visible-near-IR absorption reached its maximum after the addition of 2 equivs $TAPF_6$. The addition of the third equiv. of the oxidant led to diminished absorption in the near-IR region, in full agreement with the anodic spectroelectrochemistry (Figure 2).

Stepwise chemical oxidation of **1c** with thianthrenium hexafluorophosphate also

led to almost identical UV-vis absorption changes as observed in the course of the corresponding spectroelectrochemical experiment (Figure S7). Cyclic voltammograms in CH_2Cl_2/*n*-Bu_4NPF_6 recorded before and after the chemical oxidation of **1c** revealed the unaffected redox couples at 0.335 and 0.505 V *vs* Fc/Fc^+ (Table 1), in line with the chemical reversibility of the anodic steps on the longer time scale. The remarkably weak NIR electronic absorption between 10000-15000 cm^{-1} cm^{-1} is thus an inherent property of $\mathbf{1c}^+$, in contrast to the other divinyl diruthenium reference, $[\mathbf{1b}]^+$ (Figure S3, bottom), and a slow concomitant generation of a secondary oxidized species can be excluded.

Based on the analysis of the changes in the electronic absorption spectra in Figure 2 we propose that the lateral Ru1 and Ru2 vinyl thiophene halves of **1a** are dominantly oxidized in the initial two anodic steps, comparably with the one-electron oxidation of reference **1b**. The direct electronic interaction between the lateral parts is disrupted in the open form of the dithienyl ethene unit. The ultimate third anodic step leads to the oxidation of the central Ru3 vinyl thiophene moiety, thereby creating the two-electron-oxidized situation in each diruthenium half of the triangle, comparably with dinuclear reference $[\mathbf{1b}]^{2+}$. The evaluation of the UV-vis-NIR spectral changes complies with the cyclic voltammetric behavior and gains further support from IR spectroelectrochemical studies and DFT calculations described in the following sections.

Table 2. UV-Vis-NIR electronic absorption of ruthenium complexes **1a-1d** and their oxidation products in dichloromethane/*n*-Bu_4NPF_6.

Complex	ν_{max} (cm^{-1}) (ε_{max} (dm^3 mol^{-1} cm^{-1}))
1a	31056 (33292), 26178 (23015)
$[\mathbf{1a}]^+$	31250 (30479), 26385 (18955), 14620 (12950), 9901 (2625), 8606 (7425)
$[\mathbf{1a}]^{2+}$	31056 (27804), 27027 (14498), 14620 (25940), 9901 (5386), 8606 (14614)
$[\mathbf{1a}]^{3+}$	31056 (25331), 14410 (6018)
1b	24038 (58812)
$[\mathbf{1b}]^+$	24213 (24135), 15949 (20876), 14065 (65356), 9346 (14331), 8071 (34190)
$[\mathbf{1b}]^{2+}$	22988 (29277)
1c	29940 (20210), 26385 (16097)
$[\mathbf{1c}]^+$	30303 (18250), 17241 (1125)
$[\mathbf{1c}]^{2+}$	29673 (18875)
1d	26385 (37223)
$[\mathbf{1d}]^+$	27933 (28618), 13642 (12536), 7077 (7410), 5552 (11407)
$[\mathbf{1d}]^{2+}$	28818 (24763), 13736 (20571), 6949 (13925), 5540 (20804)
$[\mathbf{1d}]^{3+}$	27472 (19761), 10471 (31837)

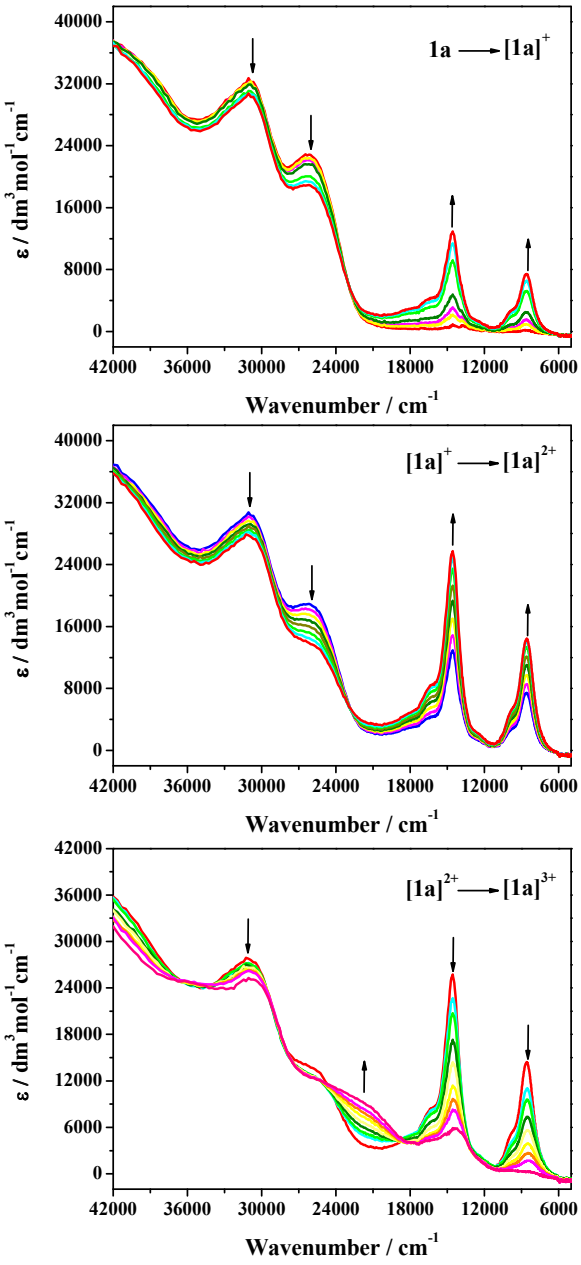

Figure 2. UV-vis-NIR spectral changes recorded during the oxidation of trinuclear complex **1a** to $[\mathbf{1a}]^{+}$ (top), $[\mathbf{1a}]^{2+}$ (middle) and $[\mathbf{1a}]^{3+}$ (bottom) in $CH_2Cl_2/10^{-1}$ M *n*-Bu_4NPF_6 at 298 K within an OTTLE cell.

IR Spectroelectrochemical Studies

Owing to the readily detectable characteristic absorption of the ethynyl moiety in

the IR region and the synergistic nature of the metal carbonyl bond, oxidation-induced shifts of the ν(C≡O) and ν(C≡C) wavenumbers for **1a-1c** and **1d**, respectively, provide an ideal spectroscopic probe through which to gauge the contribution of the bridged metal termini to the oxidation process and also to monitor directly the localized oxidations of the ethynyl terthiophene unit. Complexes **1a-1d** were oxidized within an optically transparent thin-layer electrochemical (OTTLE) cell at ambient temperature (Figure 3). The important IR spectral data are provided in Table 3.

The IR spectra of neutral di- and trinuclear ruthenium complexes **1a-1c** in CH_2Cl_2/0.1 M *n*-Bu_4NPF_6 are similar, featuring a single ν(C≡O) band at around 1922 cm^{-1}. This observation is consistent with similar electron densities at the different ruthenium sites and extent of the Ru-to-CO π-back-donation. The IR spectrum of neutral **1d** also reveals a symmetric molecular framework. Upon oxidation the ν(C≡O) band of $[\mathbf{1b}]^+$ shifted to higher energy by almost 4 cm^{-1} compared to neutral **1b**, while those of $[\mathbf{1a}]^+$, $[\mathbf{1a}]^{2+}$ and $[\mathbf{1c}]^+$ remained at almost the same positions as in the corresponding neutral complexes, manifesting a dominant involvement of the bridging ligands in the oxidation. By comparison with data reported by Winter et al. for the related diruthenium complexes,[26] the oxidation of **1b** seems to be localized slightly more on the vinyl units, affecting the Ru—CO bonds to a very limited extent, while the oxidation of **1c** is probably largely localized on the central benzothiophene part and less on the vinyl linkers. Benzothiophene in **1c** promotes the delocalization of the one-electron anodic step over the backbone, which does not happen in $[\mathbf{1a}]^+$ and $[\mathbf{1a}]^{2+}$ due to the separately redox-addressed central Ru3 vinyl thiophene segment.

Final oxidation to $[\mathbf{1a}]^{3+}$, $[\mathbf{1b}]^{2+}$ and $[\mathbf{1c}]^{2+}$ underlined interesting differences between the complexes. The intensity of the ν(C≡O) band for $[\mathbf{1c}]^{2+}$ slightly decreased, with no apparent alteration in the ν(C≡O) wavenumber, much like in the lower oxidation states.

Compared with laterally oxidized $[\mathbf{1a}]^+$ and $[\mathbf{1a}]^{2+}$, the change in the ν(C≡O) wavenumber for $[\mathbf{1a}]^{3+}$ was more perceptible and a blue shift of 2 cm^{-1} was recorded. Notably, the ^{13}C NMR spectrum of parent **1a** displays two carbonyl signals, suggesting that the Ru3 center is indeed electronically different from lateral Ru1 and

Ru2. This is also reflected in the course of the anodic path of **1a** with the first two steps residing on the lateral vinyl thiophene units and the third one mainly on the central vinyl thiophene segment.

The blue ν(C≡O) shift of 8 cm^{-1} induced by the oxidation of $[\mathbf{1b}]^{+}$ to $[\mathbf{1b}]^{2+}$ is larger compared to the initial oxidation of **1b**, showing that the second anodic step is more delocalized over the ruthenium termini. This assumption is well supported by the DFT calculations, revealing that the contribution of the ruthenium centers to the frontier redox orbitals in $[\mathbf{1b}]^{2+}$ is much larger compared to the neutral state (see Table S2).

IR monitoring of the successive oxidation of trinuclear ethynyl oligothiophene complex **1d** has been particularly informative for the allocation of the three separate anodic steps. The electrochemical generation of monocation $[\mathbf{1d}]^{+}$ and dication $[\mathbf{1d}]^{2+}$ resulted in gradual decrease (and a slight red shift) of the original ν(C≡C) band associated with neutral Ru ethynyl thiophene segments. Two new ν(C≡C) bands with lower wavenumbers appeared in the IR spectrum of $[\mathbf{1d}]^{+}$ at 1992 cm^{-1} (minor) and 1935 cm^{-1} (dominant) and their intensities further increased during the subsequent oxidation producing $[\mathbf{1d}]^{2+}$. These IR spectral changes are consistent with the localized oxidations of the lateral ethynyl thiophene moieties of **1d** breaking the original symmetry of the three C≡C bonds. It is important to note that the strong ν(C≡C) band at 1935 cm^{-1} and the remaining 'parent' ν(C≡C) band at 2051-2046 cm^{-1} reflect the 'mixed-valence' situation where the lateral ethynyl linkers bound to Ru1 and Ru2 are almost exclusively affected by the first two anodic steps while the central ethynyl linker bound to Ru3 remains largely non-oxidized in $[\mathbf{1d}]^{2+}$. The third anodic step is then the oxidation of the remaining ethynyl thiophene unit linked to the Ru3 center. The symmetric electronic arrangement of the C≡C bonds becomes indeed restored in $[\mathbf{1d}]^{3+}$, for its IR spectrum is dominated by the strongly red-shifted single ν(C≡C) band at 1910 cm^{-1}. The weak ν(C≡C) band of $[\mathbf{1d}]^{3+}$ observed at 1971 cm^{-1} most likely corresponds to a rotamer with π(C≡C) orbitals suspended to a different degree from the terthiophene core[27]. The complex $[\{Cp^*(dppe)_2Ru(-C\equiv C-)\}_2(2,2'\text{-bithiophene})]^{n+}$ (n = 0-2) as a suited diruthenium

reference[28] for **1d**, showed similar changes in the ν(C≡C) wavenumbers in its three oxidation states, providing firm evidence for the laterally localized oxidations of **1d**. Certainly, the equally similar UV-vis-NIR spectral changes of the complex $[\{Cp^*(dppe)_2Ru(-C\equiv C-)\}_2(2,2'\text{-bithiophene})]^{n+}$ (n = 0-2) is also another evidence for localized oxidations of **1d**.[28]

The detailed analysis of the oxidation evolution presented for purpose-designed **1d** strongly supports the anodic path with laterally localized individual steps proposed above for triruthenium complex **1a**. In addition, it is worth mentioning that all studied species **1a**-**1c** show only a single ν(C≡O) band in their IR spectra. Hence, the Ru(CO) termini remain electronically equivalent in all oxidation states and the spin density changes upon oxidation are dominantly localized on the conjugated vinyl thiophene redox centers (vide infra, Figure 4).[29, 30] The theoretical support for this statement is presented below in the DFT section.

Table 3. Spectroelectrochemically determined ν(C≡O) and ν(C≡C) wavenumbers (cm^{-1}) for $[\mathbf{1a}]^{n+}$-$[\mathbf{1d}]^{n+}$ (n = 0-2, and 3 for the triruthenium complexes) in dichloromethane/n-Bu_4NPF_6.

IR mode	Complex	n = 0	n = 1	n = 2	n = 3
	$[\mathbf{1a}]^{n+}$	1922s	1922s	1922s	1924s
ν(C≡O)	$[\mathbf{1b}]^{n+}$	1923s	1927s-m	1935s	--
	$[\mathbf{1c}]^{n+}$	1923s	1923s-m	1924m	--
ν(C≡C)	$[\mathbf{1d}]^{n+}$	2051m	2049m-w, 1992w, 1935 m	2046w, 1992w, 1935 s	1971vw, 1910m

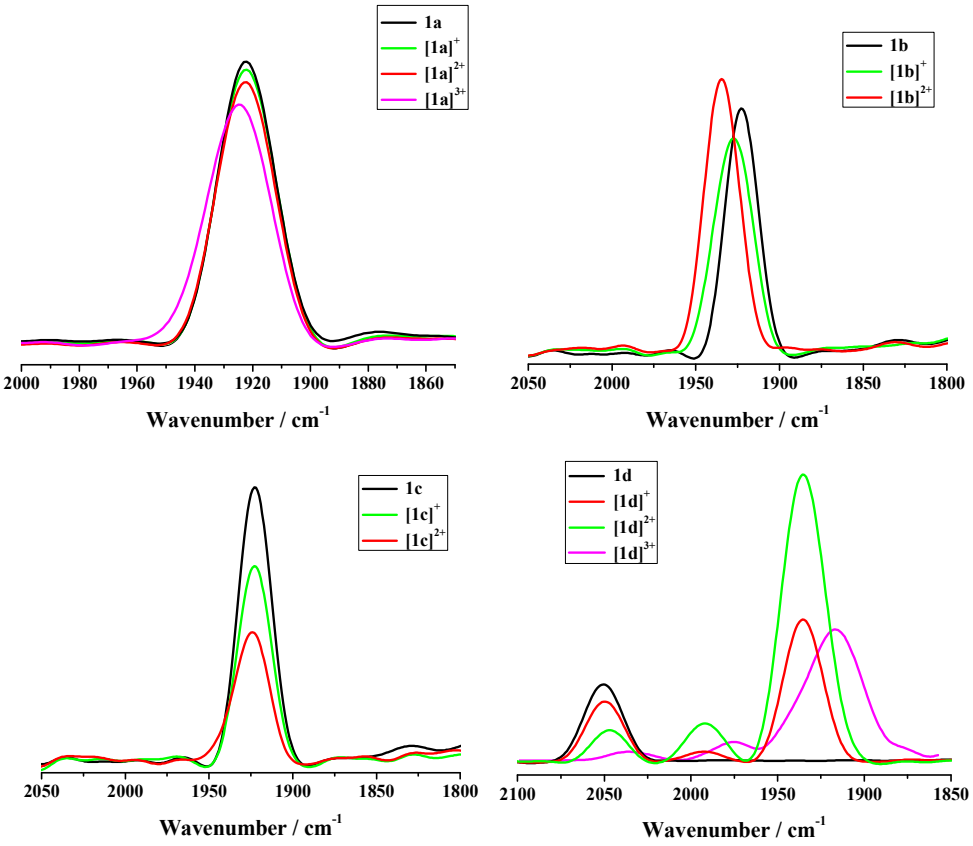

Figure 3. IR spectra recorded in the ν(C≡O) region for complexes **1a-1c** and in the ν(C≡C) region for complex **1d**, showing the wavenumber and ν(C≡C) band pattern changes for different oxidation states (0, +1, +2, +3) generated in $CH_2Cl_2/10^{-1}$ M n-Bu_4NPF_6 at 298 K within an OTTLE cell.

DFT and TD-DFT Calculations

Density functional theory (DFT) calculations were performed using the B3LYP and BLYP35 functionals to aid the description of the electronic characters of $[\mathbf{1a}]^{n+}$-$[\mathbf{1d}]^{n+}$ (n = 0-2). The basis set employed here is 6-31G* (Lanl2DZ for Ru atom). As the frameworks of these complexes are too large to be calculated efficiently, especially in the case of the triruthenium complexes, their simplified models $[\mathbf{1a\text{-}H}]^{n+}$-$[\mathbf{1d\text{-}H}]^{n+}$ (n = 0-2) were employed instead. The extension "-H" in model complexes $[\mathbf{1a\text{-}H}]^{n+}$-$[\mathbf{1d\text{-}H}]^{n+}$ (n = 0-2) means that the PMe_3 ligands in **1a-1c** have been replaced by PH_3 ligands, and the η^5-C_5Me_5 and dppe ligands in **1d** by η^5-C_5H_5

and two PH_3 ligands, respectively. Beside B3LYP, known to exaggerate delocalization, we have also employed the BLYP35 method reported by Kaupp et al.[27], which warrants a balance between localization and delocalization for mixed-valence systems. This choice is essential for symmetry-broken localized-oxidation systems, much like $\mathbf{1d}^+$ and $\mathbf{1d}^{2+}$ featuring three distinct IR ν(C≡C) absorption bands. In order to account for also solvent effects, the conductor polarizable continuum model (CPCM) in CH_2Cl_2 has been employed for ground state structure optimizations and analyses of $[\mathbf{1a\text{-}H}]^{n+}$-$[\mathbf{1d\text{-}H}]^{n+}$ (n = 0-2) as well as in TD-DFT calculations of their electronic excitation energies. The selected frontier orbitals are shown in Figure 5, Figures S8-S11 and Figures S13-S14 (Supporting Information). Lists of frontier molecular orbital energies and compositions for [**1a-H**]-[**1d-H**] from the Mulliken analysis are provided in Tables S1-S3 (Supporting Information).

As shown in Figures S8-S11 and Tables S1-S3, DFT calculations (both B3LYP and BLYP35) show the HOMO and HOMO-1 of neutral [**1b-H**] and [**1c-H**] delocalized across the entire metal-organic π system, with contributions of 6% ([**1b-H**] and **[1c-H**]) from the ruthenium centers and up to 80% from the bridging moieties. In contrast, the HOMO-1 of the triruthenium complexes [**1a-H**] and [**1d-H**] weigh heavily on one side of the molecular framework, featuring strongly uneven lateral distributions resembling [**1b-H]**. On the other hand, the HOMO contours are still fairly symmetrical.

With regard to one-electron-oxidized $[\mathbf{1a\text{-}H}]^+$-$[\mathbf{1d\text{-}H}]^+$, the spin density distribution (Figure 4 and Figure S12) and the ν(C≡O) and ν(C≡C) wavenumbers calculated within the harmonic approach (Table S4) with the two different methods (B3LYP and BLYP35) have shown no obvious difference. The spin densities in all the complexes are distributed dominantly over the central molecular backbone with only minor contributions from the metal centers. The large involvement of the bridge confirms the redox non-innocent character of the ligands. However, in terms of comparative analysis of the ruthenium-vinyl complexes $[\mathbf{1a\text{-}H}]^+$-$[\mathbf{1c\text{-}H}]^+$, the spin density distribution reveals some differences between the three singly oxidized complexes. The share from the bridge core in $[\mathbf{1b\text{-}H}]^+$ is slightly smaller than that in

[**1a-H**]$^+$ and [**1c-H**]$^+$, probably due to a lower degree of conjugation in the dithiophene portion ([**1b-H**]$^+$) compared to the terthiophene ([**1a-H**]$^+$) and benzothiophene ([**1c-H**]$^+$) moieties. The spin density in [**1c-H**]$^+$ concentrates almost entirely on the dithienyl pentene moiety, confirming an almost fully bridge-localized oxidation process. On the whole, the oxidation behavior of diruthenium complexes **1b**$^+$ and **1c**$^+$ complies with other reported cases of this kind of compounds.[2-8, 17, 31] Some appropriate asymmetric spin density distributions has been calculated for [**1d-H**]$^+$, the spin density being weighed heavily on one of the lateral parts of the central triangular linker. This observation further verifies the preferential lateral oxidization of **1d** along the first two anodic steps, as revealed by the UV-vis-NIR and IR spectroelectrochemical monitoring. The experimental anodic behavior of **1a** with the vinyl instead of ethynyl linkers is identical (Figures 2 and S5); however, even the BLYP35 method exaggerates the fairly symmetrical distribution of the spin density over all three redox centers in [**1a-H**]$^+$. The laterally localized oxidation of **1a** then obtains a convincing support from diruthenium reference **1b** (almost identical NIR spectral changes seen in Figure 2 and Figure S3) and model [**1b-H**]$^+$ calculated with BLYP35 that reveals an asymmetric distribution of the spin density (Figure 4).

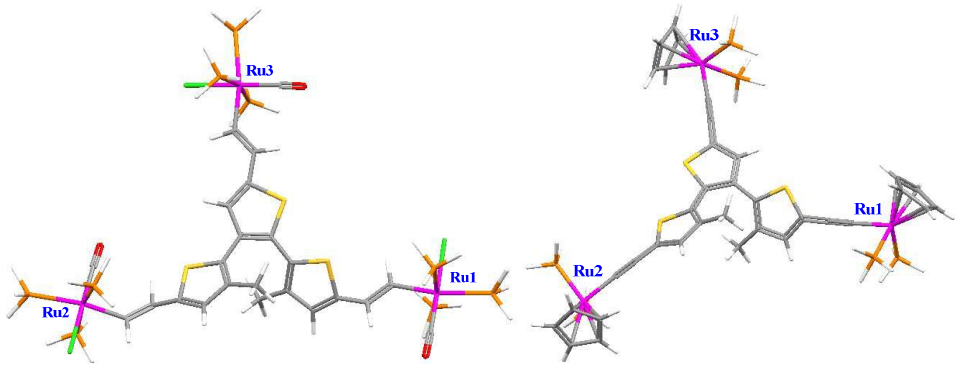

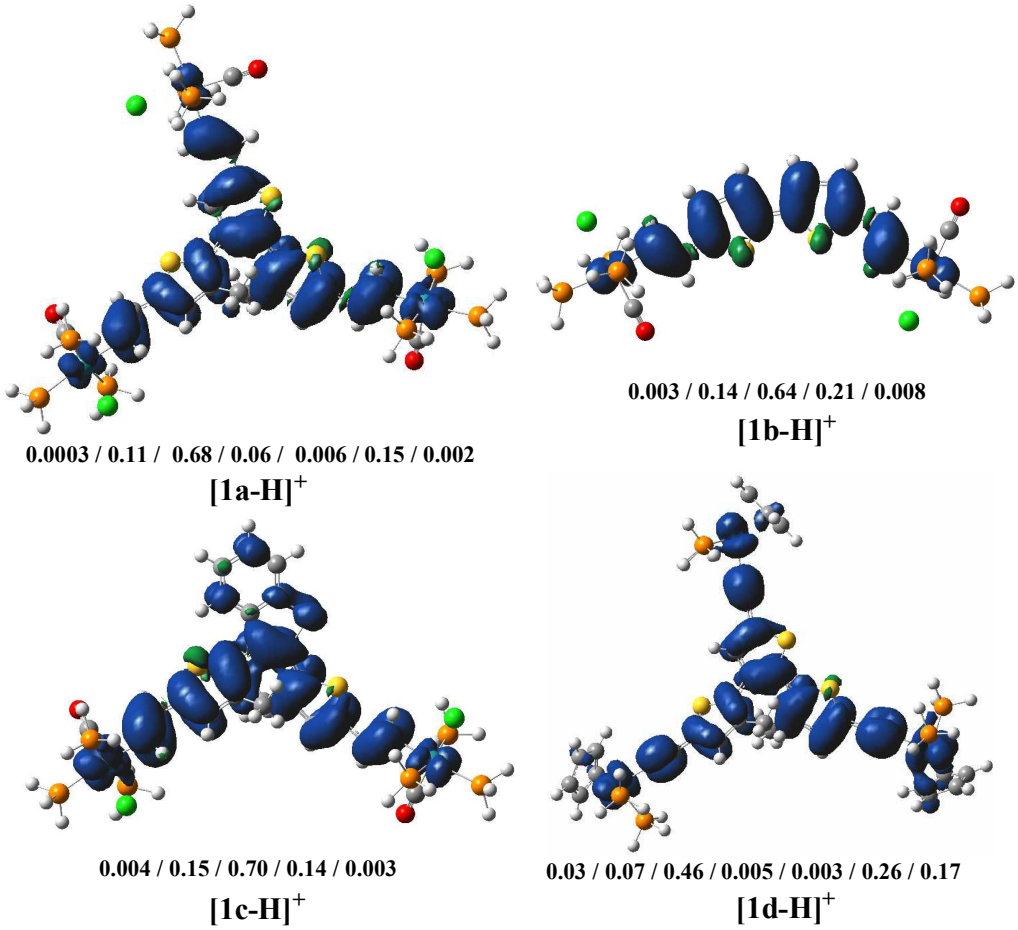

Figure 4. Spin density distribution in [**1a-H**]$^+$ (Ru2/CH=CH/oligothiophene /CH=CH/Ru3/CH=CH/Ru1), [**1b-H**]$^+$ and [**1c-H**]$^+$ (Ru/CH=CH/oligothiophene/CH=CH/Ru), and [**1d-H**]$^+$ (Ru2/CH≡CH/oligothiophene/CH≡CH/Ru3/CH≡CH/Ru1). Contour values: ±0.04 (e/bohr^3)$^{1/2}$. BLYP35/6-31G* (Ru: Lanl2DZ)/CPCM /CH_2Cl_2. The model structures of parent [**1a-H**] and [**1d-H**] are shown in the top.

To aid the assignment of the electronic absorptions in the oxidized complexes, the nature of the electronic transitions was explored by time-dependent (TD) DFT calculations on the models, viz.[**1a-H**]$^+$-[**1d-H**]$^+$ and [**1a-H**]$^{2+}$, [**1d-H**]$^{2+}$ (Figure 5, and Figures S13 and S14). The predicted major electronic excitations with oscillator strength (f), dominant configuration contribution, and assignment are shown in Tables 4 and S5-S6. For [**1c-H**]$^+$, the simulations of the absorption in the NIR region resulting from both methods (B3LYP and BLYP35) are not consistent with the very weak NIR absorption in the recorded experimental spectrum of [**1c**]$^+$ (Figures S4 and

S7). This discrepancy probably reflects the fact that the DFT calculations exaggerate the delocalization and the true oxidation of **1c** is more benzothiophene-localized than in the calculated system. Stepping back to make a comparison between these two methods, B3LYP and BLYP35, judging by the consistency of the results calculated by two methods with the experimental data, the latter method was less accurate for having failed to reproduce the NIR absorption of [**1b**]$^+$ (Tables S5 and S6). In good agreement with the main bands observed experimentally, the intense doublet excitations obtained by the B3LYP method, especially the low-energy absorptions in the NIR region, have been well predicted for models [**1a-H**]$^+$ and [**1d-H**]$^+$ (for the former: D_1, D_2 and D_3; for the latter: D_1, D_2 and D_9, Table 4 and Figure 5). It should be noted that the molecular spectroscopic absorption data obtained with the BLYP35 method show obvious flaws compared to the experimental results. Consequently, a detailed discussion of the electronic absorption spectra of [**1a-H**]$^+$ and [**1d-H**]$^+$ has been based on the results obtained with the B3LYP method for the sake of brevity (Table 4 and Figure 5). The lower-energy excitations at 1571 nm (6365 cm^{-1}) and 992 nm (10080 cm^{-1}) calculated for [**1a-H**]$^+$ are associated with β-HOSO→β-LUSO and β-HOSO-1→β-LUSO excitations, respectively, both being attributed to intra-ligand π→π* transitions with some admixed metal-to-ligand (ML) CT character. The same assignment applies for the NIR absorption bands of complex [**1d-H**]$^+$ at 1924 nm (10834 cm^{-1}) and 1342 nm (7451 cm^{-1}), belonging again to β-HOSO→β-LUSO and β-HOSO-1→β-LUSO electronic transitions, respectively. Therefore, there are no real mixed-valence Ru(II)-Ru(III) states in **1a**$^+$ and **1d**$^+$ (in line with the reference absorption of **1b**$^+$) and the singly oxidized triruthenium species exhibit only very limited Ru(II)-to-bridge(+) charge transfer character of the lowest optically populated excited states. As shown in Figure 5, it is worth noting that we can also seize very important information about the electronic transport path according to different electron distributions. The singly occupied orbitals β-HOSO and β-HOSO-1 for [**1a-H**]$^+$ and [**1d-H**]$^+$ all weigh heavily on one side of the symmetric structures (seriously unbalanced distributions), similar to those of the corresponding HOMO-1 orbitals, while the homologous orbitals for reference [**1b-H**]$^+$ are strongly balanced on

both sides of the molecule, comparably with HOMO and HOMO-1 in parent [**1b-H**]. Furthermore, we have been able to reproduce the peculiar absorptions of the biradical singlet and triplet states in $[\mathbf{1a\text{-}H}]^{2+}$ and $[\mathbf{1d\text{-}H}]^{2+}$ with the aid of the relatively suited B3LYP method used to discuss the mono-cationic data (Table 4). By comparison, we find that the simulated absorptions for the triplet (biradical) states for $[\mathbf{1a\text{-}H}]^{2+}$ and $[\mathbf{1d\text{-}H}]^{2+}$ are more consistent with the experimental results than those of the singlets, which further confirms the identical vis-NIR absorptions seen both for the monocations and dications of **1a** and **1d** with identical chromophores and low-energy electronic transitions (Figures 2 and S14).

Table 4. Major electronic excitations in $[\mathbf{1a\text{-}H}]^{+}$, $[\mathbf{1a\text{-}H}]^{2+}$ and $[\mathbf{1d\text{-}H}]^{+}$, $[\mathbf{1d\text{-}H}]^{2+}$ determined by TD-DFT methods.[a]

Complex	Excited state	λ/nm [cm^{-1}]	Osc. str (f)	Major contributions	Assignment
$[\mathbf{1a\text{-}H}]^{+}$	D_1	1571 [6365]	0.2098	β-HOSO→β-LUSO (99%)	bridge π–π* / MLCT
	D_2	992 [10080]	0.3952	β-HOSO-1→β-LUSO (97%)	bridge π–π* / MLCT
	D_3	604 [16556]	0.3760	β-HOSO-9→β-LUSO (77%)	bridge π–π*
$[\mathbf{1a\text{-}H}]^{2+}$	S_1	1169 [8554]	0.4997	HOMO→LUMO (72%)	bridge π–π* / MLCT
	S_2	743 [13458]	0.2484	HOMO-1→LUMO (70%)	bridge π–π* / MLCT
	T_1	1632 [6127]	0.0992	β-HOSO→β-LUSO (99%)	ILCT/ MLCT/ LMCT
	T_2	1039 [9624]	0.4104	β-HOSO→β-LUSO (97%)	ILCT / MLCT/ LMCT
$[\mathbf{1d\text{-}H}]^{+}$	D_1	1924 [5197]	0.2303	β-HOSO→β-LUSO (97%)	bridge π–π*/ MLCT
	D_2	1342 [7451]	0.5451	β-HOSO-1→β-LUSO (99%)	MLCT/ bridge π–π*
	D_9	630 [15873]	0.4010	β-HOSO-9→β-LUSO (73%)	MLCT

[**1d-H**]$^{2+}$	S_1	1377 [7262]	0.5758	HOMO→LUMO (73%)	MLCT/ bridge π–π*
	S_4	875 [11428]	0.9671	HOMO-1→LUMO (57%)	MLCT/ bridge π–π*
	T_1	2311 [4327]	0.1041	β-HOSO→β-LUSO (100%)	ILCT/ MLCT/ LMCT
	T_2	1401 [7137]	0.4138	β-HOSO→β-LUSO (86%)	ILCT / MLCT/ LMCT

[a] The computation method is B3LYP / 6-31G* (Ru: Lanl2DZ) / CPCM / CH_2Cl_2. *D* = doublet, *S* = singlet, *T* = triplet.

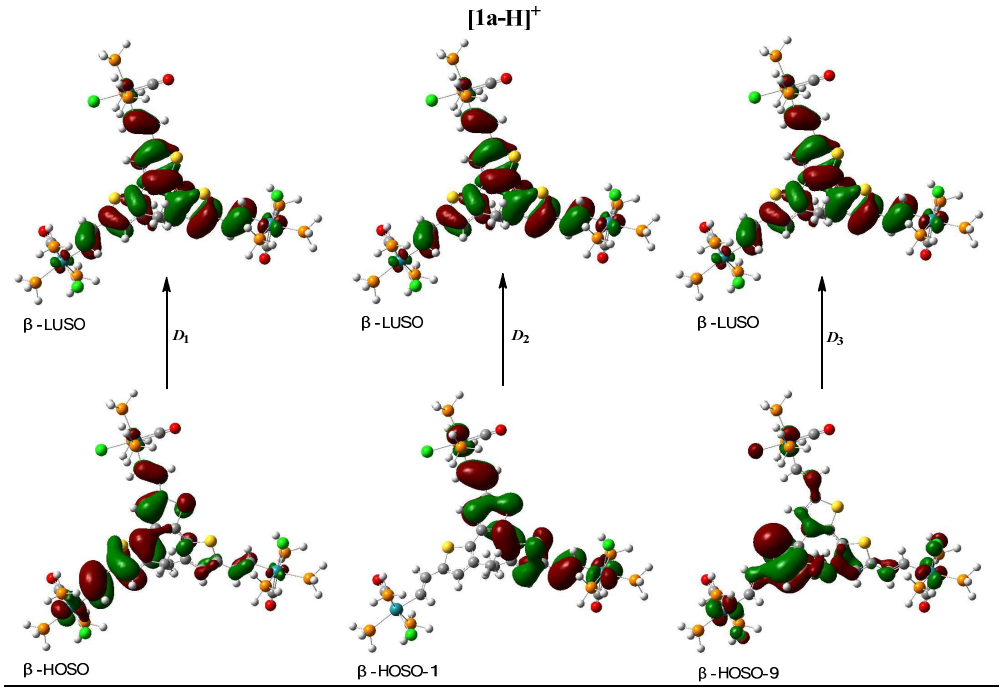

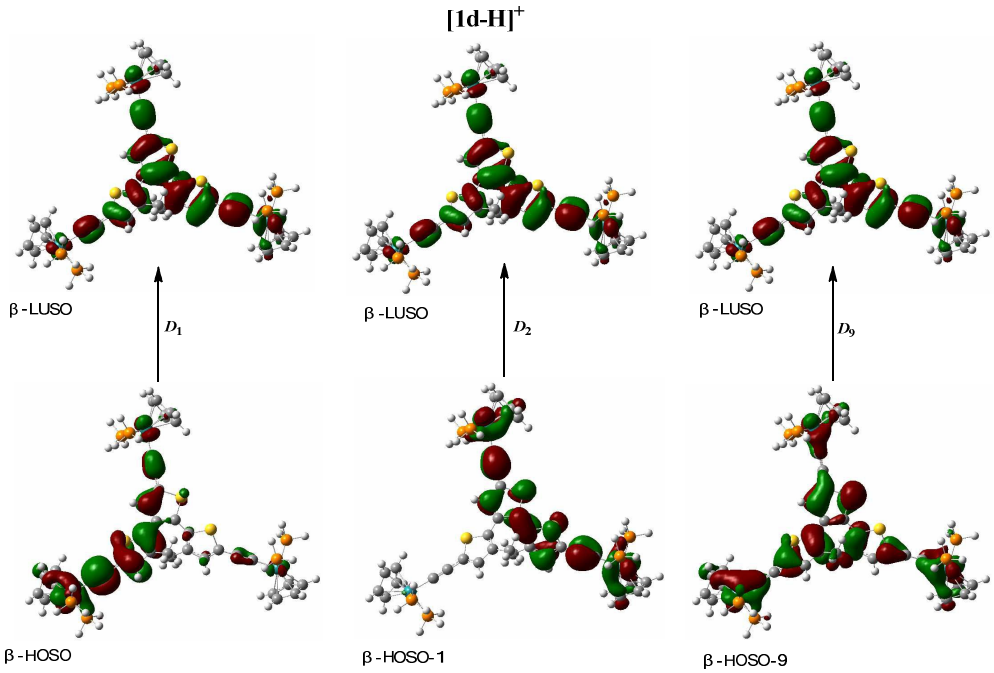

Figure 5. Spin orbitals involved in the major electronic excitations in [**1a-H**]$^+$ and [**1d-H**]$^+$ shown in **Table 4** (*D* = doublet). B3LYP / 6-31G* (Ru: Lanl2DZ) / CPCM / CH_2Cl_2.

With respect to the vibrational frequency calculations, complexes [**1a-H**]$^+$-[**1c-H**]$^+$ all exhibit a single intense ν(C≡O) band (BLYP35: around 2261 cm^{-1}; B3LYP: around 1965 cm^{-1}, scaled by 0.95 and 0.9614 for BLYP35 and B3LYP, respectively, see the Computational Details), which matched the sole-peak features observed experimentally in the IR spectroelectrochemistry course (Table S4). The ν(C≡C) band pattern of [**1d**]$^+$ (1935 (s), 1992 (w), 2049 (m-w)) is reproduced basically for [**1d-H**]$^+$ by both computational methods (Table S4, B3LYP: 1980 (s), 2001 (m) and 2046 cm^{-1} (w); BLP35: 2255 (s), 2270 (m) and 2298 cm^{-1} (w)). The simulation of the peak intensity pattern using the B3LYP method is still flawed; specifically, the intensity of calculated bands at 2001 cm^{-1} is exaggerated, which may belong to the 'non-oxidized' lateral linker segment feeling the oxidation somewhat because the DFT exaggerates delocalization. The ν(C≡O) or ν(C≡C) wavenumbers have also been calculated for neutral [**1a-H**]-[**1d-H**] and dications [**1a-H**]$^{2+}$-[**1d-H**]$^{2+}$ using the two methods (Table S4, scaled by 0.95 and 0.9614 for BLYP35 and B3LYP, respectively, see the Computational Details). Likewise, we have presented the data of

[**1a-H**]$^{2+}$ and [**1d-H**]$^{2+}$ under the singlet and triplet states using the B3LYP method (Table S4). It is remarkable that the DFT data for [**1a-H**]$^{2+}$ show three (BLYP35) or two (B3LYP) close-lying ν(C≡O) bands, differently from **1a**$^{2+}$ where the Ru(CO) centers have been excluded from the anodic processes. On the other hand, a single ν(C≡O) or ν(C≡C) absorption band was calculated for the symmetric diruthenium model complexes. Finally, [**1d-H**]$^{2+}$ again strongly relates to [**1d-H**]$^{+}$. The calculated ν(C≡O) shifts are larger than those observed in the experiments, indicating that the DFT calculations indeed exaggerate the delocalization of the oxidation effects over the vinyl-Ru(CO) moiety. The $\Delta\nu$ values for the ν(C≡C) modes corresponding to the one-electron and two-electron oxidations of [**1d-H**] are consistent with the experimental data, although the oxidations of **1d** are actually more laterally localized than in the calculated oxidation products.

It must be noted that various mutual orientations of the ligated metal termini and the bridging moieties have a significant impact on the charge delocalization and localization in the mixed-valence systems.[23c, 27c, 27d, 32] We have employed the simplified models of all the studied complexes without involving the conformational effect to a certain extent, as the frameworks of our system are too large to be calculated efficiently. Nevertheless, the presented theoretical results provide convincing support to the localized oxidation processes for the first two anodic steps of **1a** and **1d**.

Conclusions

This work presents a series of dinuclear and trinuclear ruthenium complexes **1a-1d** bridged by vinyl/ethynyl oligothiophene ligands. A convenient combination of cyclic voltammetry (CV), square wave voltammetry (SWV), *in situ* IR and UV-vis-NIR spectroelectrochemistry and DFT/TDDFT calculations proved to be a powerful tool to unravel the peculiar electrochemical, spectroscopic and electronic bonding properties of these compounds in different oxidation states. The electrochemical and UV-vis-NIR spectroelectrochemical results consistently reveal

that the first two anodic steps observed for **1a** are largely localized on the lateral framework (the Ru1 or Ru2 vinyl thiophene moieties), based on the reasonable evidence from the related data recorded for diruthenium references **1b** and **1d**. The analysis of IR ν(C≡C) absorption bands for $[\mathbf{1d}]^{+}$, $[\mathbf{1d}]^{2+}$ and $[\mathbf{1d}]^{3+}$ reveals that the lateral ethynyl linkers bound to Ru1 and Ru2 are almost exclusively affected by the first two anodic steps, while the third anodic step involves the remaining Ru3 ethynyl thiophene unit. The hardly perceptible changes in the *ν*(C≡O) wavenumber of **1a** on oxidation combined with the distinct evolution of the *ν*(C≡C) absorption bands of **1d** confirm the dominantly bridge-localized oxidation of the triruthenium complexes, which is further confirmed to a large extent by the DFT and TD-DFT calculations. The existence of Ru(II)-Ru(III) mixed-valence states in the monocations and dications of **1a** and **1d** has been excluded. Instead, the oxidized species show intense π-π* ILCT transitions in the NIR region admixed with some MLCT character. The description of these characteristic processes adds a new piece of knowledge to the understanding of electron-transfer processes in coordination compounds featuring conjugated multiple redox sites.

Experimental Section

General Materials

All manipulations were carried out under a dry argon gas atmosphere by using standard Schlenk techniques, unless stated otherwise. Solvents were pre-dried and distilled under argon prior to use, except those used directly for spectroscopic measurements, which were of spectroscopic grade. The starting materials **2a** (ref.[33]), **2c** (ref.[34]), **2b** (ref.[35]), $[Pd(PPh_3)_4]$ (ref.[36]), $[RuHCl(CO)(PPh_3)_3]$ (ref.[37]) and $[RuCl(\eta^5\text{-}C_5Me_5)(dppe)]$ (ref.[38]) were prepared by the respective procedures described in the literature. Target complexes **1a-d** were prepared according to the synthetic route presented in Scheme 1. Other reagents were purchased and used as received.

*Syntheses of Intermediate Compounds **3a** and **3c***

Synthesis of **3a**: To a stirred solution of **2a** (2.43 g, 5 mmol), CuI (0.14 g, 0.75 mmol), and [$Pd(PPh_3)_4$] (0.058 g, 0.5 mmol) in triethylamine (50 mL) and toluene (100 mL) under a dry argon gas atmosphere, trimethylsilyl acetylene (10 mL, 75 mmol) was added, and the mixture was refluxed at 60 °C for 24 h. The cold solution was filtered through a bed of Celite 545. The filtrate was evaporated under reduced pressure and purified by silica gel column chromatography (petroleum ether/dichloromethane 5:1, v/v) to give a yellow solid (2.61 g, 77%).

Compound **3a**: ^{1}H NMR (400 MHz, $CDCl_3$): δ 0.23 (s, 9H, $SiCH_3$), 0.24 (s, 9H, $SiCH_3$), 0.26 (s, 9H, $SiCH_3$), 1.88 (s, 3H, CH_3), 1.96 (s, 3H, CH_3), 6.95 (s, 1H, thiophene-H), 6.96 (s, 1H, thiophene-H), 7.18 (s, 1H, thiophene-H). ^{13}C NMR (100 MHz, $CDCl_3$): δ 0.2, 14.4, 14.8, 96.4, 97.1, 97.4, 99.5, 100.3, 101.0, 122.2, 123.1, 123.3, 130.1, 131.9, 132.6, 133.5, 135.4, 135.1, 135.6, 135.8, 136.7. MS (*m/z*): 564.18 (M^+). Anal. Calcd for $C_{29}H_{36}S_3Si_3$: C, 61.64; H, 6.42. Found: C, 61.53; H, 6.39.

Synthesis of **3c**: The procedure for **3c** was similar to that for **3a**, using the compound **2c** (2.40 g, 5 mmol) instead of **2a**. Yield: 1.78 g (69%) of a yellow solid.

Compound **3c**: ^{1}H NMR (400 MHz, $CDCl_3$): δ 0.26 (s, 9H, $SiCH_3$), 0.28 (s, 9H, $SiCH_3$), 1.90 (s, 3H, CH_3), 2.11 (s, 3H, CH_3), 6.99 (s, 1H, thiophene-H), 7.11 (s, 1H, thiophene-H), 7.38-7.40 (m, 2H, Ar), 7.61-7.64 (m, 1H, Ar), 7.83-7.85 (m, 1H, Ar). ^{13}C NMR (100 MHz, $CDCl_3$): δ 0.2, 14.5, 15.1, 97.2, 97.5, 99.5, 100.3, 121.9, 123.1, 123.5, 123.8, 124.9, 125.2, 127.0, 130.9, 131.6, 134.4, 135.6, 135.9, 136.8, 137.0, 139.0, 139.7. MS (*m/z*): 518.26 (M^+). Anal. Calcd for $C_{28}H_{30}S_3Si_2$: C, 64.81; H, 5.83. Found: C, 64.95; H, 5.88.

*Syntheses of Intermediate Compounds **4a** and **4c***

Synthesis of **4a**: A mixture of **3a** (1.5 g, 2.6 mmol) and potassium hydroxide (0.55 g, 9.5 mmol) were stirred at room temperature for 2 h in a mixture of THF and methanol (30 mL, 1/1, v/v) under nitrogen atmosphere. The reaction mixture was diluted with dichloromethane and washed with brine. The combined organic layers were dried (Na_2SO_4) and the solvent was removed in vacuum. The compound was purified by column chromatography (petroleum ether/dichloromethane 6:1, v/v) and

obtained as yellow oil in 90% yield (0.83 g).

Compound **4a**: ^{1}H NMR (400 MHz, $CDCl_3$): δ 1.91 (s, 3H, CH_3), 1.98 (s, 3H, CH_3), 3.35 (s, 1H, C≡CH), 3.37 (s, 1H, C≡CH), 3.44 (s, 1H, C≡CH), 6.98 (s, 1H, thiophene-H), 6.99 (s, 1H, thiophene-H), 7.24 (s, 1H, thiophene-H). ^{13}C NMR (100 MHz, $CDCl_3$): δ 14.4, 14.7, 75.9, 76.5, 76.8, 82.0, 82.6, 83.2, 121.2, 122.1, 122.2, 130.0, 131.9, 132.6, 133.7, 135.6, 135.7, 135.9, 136.1, 136.9. MS (*m/z*): 348.00 (M^+). Anal. Calcd for $C_{20}H_{12}S_3$: C, 68.93; H, 3.47. Found: C, 68.89; H, 3.48.

Synthesis of **4c**: The procedure for **4c** was similar to that for **4a**, using the compound **3c** (1.35 g, 2.6 mmol) instead of **3a** and potassium hydroxide (0.39 g, 6.8 mmol). Yield: 0.91 g (93%) of a yellow solid.

Compound **4c**: ^{1}H NMR (400 MHz, $CDCl_3$): δ 1.89 (s, 3H, CH_3), 2.11 (s, 3H, CH_3), 3.35 (s, 1H, C≡CH), 3.37 (s, 1H, C≡CH), 6.99 (s, 1H, thiophene-H), 7.12 (s, 1H, thiophene-H), 7.36 (t, J_{HH} = 4 Hz, 2H, Ar), 7.59 (t, J_{HH} = 4 Hz, 1H, Ar), 7.81 (t, J_{HH} = 4 Hz, 1H, Ar). ^{13}C NMR (100 MHz, $CDCl_3$): δ 14.5, 15.1, 76.6, 76.9, 82.0, 82.6, 121.9, 122.0, 122.5, 123.5, 124.9, 125.3, 127.0, 131.1, 131.7, 134.3, 135.9, 136.1, 136.2, 136.8, 137.1, 139.0, 139.6. MS (*m/z*): 374.05 (M^+). Anal. Calcd for $C_{22}H_{14}S_3$: C, 70.55; H, 3.77. Found: C, 70.63; H, 3.80.

*Syntheses of Target Metal Complexes **1a-1d***

Synthesis of **1a**: A solution of **4a** (0.08 g, 0.25 mmol) in CH_2Cl_2 (7 mL) was slowly added to a suspension of [$RuHCl(CO)(PPh_3)_3$] (0.71 g, 0.75 mmol) in CH_2Cl_2 (7 mL) . The reaction mixture was stirred for 12 h to give a red solution. Then, 1 M PMe_3 in THF (3 mL, 3 mmol) was added and the mixture was stirred for another 24 h. The solution volume was reduced to ca. 2 mL under vacuum. Addition of hexane (30 mL) to the residue produced a yellow solid that was collected by filtration, washed with hexane, and dried under vacuum. Yield: 0.20 g (53%).

Complex **1a**: ^{1}H NMR (400 MHz, $CDCl_3$): δ 1.38 (m, 36H, PMe_3), 1.42 (m, 18H, PMe_3), 1.47 (m, 27H, PMe_3), 1.80 (s, 3H, CH_3), 2.01 (s, 3H, CH_3), 6.31 (s, 1H, thiophene-H), 6.40 (s, 1H, thiophene-H), 6.58-6.61 (m, 4H, thiophene-H (1H), thiophene-CH= (3H)), 7.53-7.83 (m, 3H, RuCH=). ^{13}C NMR (100 MHz, $CDCl_3$): δ

14.7, 14.8, 16.4, 16.6, 16.7, 18.7, 19.8, 20.1, 120.3, 121.1, 121.4, 126.6, 127.8, 128.2, 128.8, 129.3, 132.2, 133.7, 134.1, 134.9, 145.6, 147.5, 147.8, 163.4, 166.5, 202.1, 202.3. ^{31}P NMR (160 MHz, $CDCl_3$): δ -19.57 (t, J = 31.9 Hz), -7.92 ~ -7.79 (m). Anal. Calcd for $C_{50}H_{98}Cl_3O_3P_9Ru_3S_3$: C, 39.20; H, 6.45. Found: C, 38.89; H, 6.48.

Syntheses of **1b** and **1c**: The procedure for **1b** and **1c** was similar to that for **1a**, using [RuHCl(CO)(PPh_3)$_3$] (0.48 g, 0.5 mmol), **2b** (0.05 g, 0.25 mmol) or **4c** (0.09 g, 0.25 mmol) instead of **4a**. Yield: 0.18 g (71%) of a brick red solid (**1b**) and 0.17 g (57%) of a yellow solid (**1c**).

Complex **1b**: ^{1}H NMR (400 MHz, $CDCl_3$): δ 1.40 (t, J_{HP} = 3.2 Hz, 36H, PMe_3), 1.47 (d, J_{HP} = 3.4 Hz, 18H, PMe_3), 6.44 (d, J_{HH} = 1.4 Hz, 2H, thiophene-H), 6.45-6.66 (m, 2H, thiophene-CH=), 6.89 (d, J_{HH} = 1.8 Hz, 2H, thiophene-H), 7.78-7.84 (m, 2H, RuCH=). ^{13}C NMR (100 MHz, $CDCl_3$): δ 16.5, 16.5, 16.6, 19.9, 19.9, 128.5, 131.8, 137.3, 149.2, 166.6, 167.9, 202.2. ^{31}P NMR (160 MHz, $CDCl_3$): δ -20.85 (t, J = 20.16 Hz), -9.12 (d, J = 21.6 Hz). Anal. Calcd for $C_{32}H_{64}Cl_2O_2P_6Ru_2S_2$: C, 38.29; H, 6.43. Found: C, 38.17; H, 6.29.

Complex **1c**: ^{1}H NMR (400 MHz, $CDCl_3$): δ 1.39-1.43 (m, 36H, PMe_3), 1.45-1.47 (m, 18H, PMe_3), 1.80 (s, 3H, CH_3), 1.91 (s, 3H, CH_3), 6.38 (s, 1H, thiophene-H), 6.44 (s, 1H, thiophene-H), 6.53-6.68 (m, 2H, thiophene-CH=), 7.26-7.33 (m, 3H, Ar (2H), RuCH= (1H)), 7.76-7.82 (m, 3H, Ar (2H), RuCH= (1H)). ^{13}C NMR (100 MHz, $CDCl_3$): δ 14.0, 14.8, 15.1, 15.66, 15.7, 16.5, 16.7, 16.8, 17.7, 18.4, 18.8, 19.0, 19.9, 20.1, 22.6, 120.9, 123.7, 124.1, 125.3, 127.8, 128.4, 128.4, 128.6, 129.4, 131.9, 133.6, 134.0, 136.7, 137.2, 140,5, 149.2, 166.0, 166.8, 167.8, 168.5, 202.2, 203.4. ^{31}P NMR (160 MHz, $CDCl_3$): δ -19.53 (t, J = 33.8 Hz), -7.83 ~ -6.39 (m). Anal. Calcd for $C_{42}H_{72}Cl_2O_2P_6Ru_2S_3$: C, 43.33; H, 6.23. Found: C, 43.37; H, 6.28.

Synthesis of **1d**: A mixture of **4a** (0.1 g, 0.3 mmol), [RuCl(η^5-C_5Me_5)(dppe)] (0.64 g, 0.96 mmol) and Na[BPh_4] (0.34 g, 2.7 mmol) was stirred for 0.5 h in THF/Et_3N 1:1 (v/v, 30 mL) under a nitrogen atmosphere. Then DBU (1,8-diazabicyclo[5.4.0]undec-7-ene) (2 mL) was added and the mixture was refluxed for 48 h. The crude product was purified by column chromatography on neutral

alumina by elution with petroleum ether/acetone 3:1 (v/v) and recrystallized from dichloromethane/ *n*-hexane to give a yellow solid. Yield: 270 mg (40%).

Complex **1d**: ^{1}H NMR (400 MHz, $CDCl_3$): δ 1.53 (s, 30H, Cp*), 1.56-1.66 (m, 21H, Cp*(15H), CH_3 (6H)), 1.77-1.95 (m, 6H, CH_2), 2.60-2.61 (m, 6H, CH_2), 7.20-7.40 (m, 50H, Ar), 7.72-7.78 (m, 13H, Ar). ^{13}C NMR (100 MHz, $CDCl_3$): δ 10.0, 14.0-14.7, 25.6, 29.3-29.7, 67.9, 92.5, 92.7, 101.4, 127.0, 127.3, 128.9, 133.2, 136.3-136.8, 138.4-138.8. ^{31}P NMR (160 MHz, $CDCl_3$): δ 78.25 (s). Anal. Calcd for $C_{129}H_{129}P_6Ru_3S_3$: C, 68.42; H, 5.74. Found: C, 68.37; H, 5.63.

Physical Measurements

^{1}H, ^{13}C, and ^{31}P NMR spectra were collected on a Varian Mercury Plus 400 spectrometer (400 MHz). ^{1}H and ^{13}C NMR chemical shifts are relative to TMS, and ^{31}P NMR chemical shifts to 85% H_3PO_4. Elemental analyses (C, H, N) were performed with a Vario ElIII Chnso instrument. The electrochemical measurements were performed on a CHI 660C potentiostat (CHI USA). A three-electrode single-compartment cell was used for the solution of complexes and supporting electrolyte in dry CH_2Cl_2. The solution was deaerated by argon bubbling on a frit for about 10 min before the measurement. The analyte (complex, ligand) and electrolyte (*n*-Bu_4NPF_6) concentrations were typically 10^{-3} and 10^{-1} mol dm^{-3}, respectively. A 500-μm diameter platinum disk working electrode, a platinum wire counter electrode, and an Ag/Ag^{+} reference electrode were used. Spectroelectrochemical experiments at room temperature were performed with an airtight optically transparent thin-layer electrochemical (OTTLE) cell (optical path length of ca 200 μm) equipped with a Pt minigrid working electrode and CaF_2 windows[39]. The cell was positioned in the sample compartment of a Bruker Tensor FT-IR spectrometer (1 cm^{-1} spectral resolution, 8 scans) or a Shimadzu UV-3600 UV-vis-NIR spectrophotometer. The controlled-potential electrolyses were carried out with a CHI 660C potentiostat. The sample concentration was ca 2×10^{-3} mol dm^{-3}, and 10^{-1} M *n*-Bu_4NPF_6 was used as the supporting electrolyte. Complexes **1a-1d** were oxidized stepwise, by increasing the anodic potentials in steps of 10, 20, or 30 mV.

Computational Details

DFT calculations were performed with the Gaussian 09 program[40], at the B3LYP/6-31G* and BLYP35 (ref.[41])/6-31G* levels of theory. Geometry optimizations were performed without any symmetry constraints, and frequency calculations on the resulting optimized geometries showed no imaginary frequencies. Electronic transitions were calculated by the time-dependent DFT (TD-DFT) method. The MO contributions were generated using the Multiwfn2.6.1_bin_Win package and plotted using GaussView 5.0. The solvation effects in dichloromethane are included for all the calculations with the conductor polarizable continuum model (CPCM)[42]. Calculated harmonic vibrational frequencies were scaled by an empirical factor of 0.95 (BLYP35) and 0.9614 (B3LYP).[43, 44]

Acknowledgements

The authors acknowledge financial support from National Natural Science Foundation of China (21272088, 21472059, 21402057) and the self-determined research funds of CCNU from the colleges' basic research and operation of MOE (CCNU14A05009, CCNU14F01003).

Author Information

[a] *Key Laboratory of Pesticide & Chemical Biology, Ministry of Education, College of Chemistry, Central China Normal University, 152 Luoyu Road, Wuhan, Hubei 430079 (China)*

E-mail: chshliu@mail.ccnu.edu.cn (S. H. Liu); f.hartl@reading.ac.uk (F. Hartl)

Notes

The authors declare no competing financial interest.

† **Electronic supplementary information (ESI) available:** Electrochemistry, UV-vis-NIR and IR spectroelectrochemistry, DFT data.

References

1 (a) M. A. Fox, R. L. Roberts, T. E. Baines, B. Le Guennic, J.-F. Halet, F. Hartl, D. S. Yufit, D. Albesa-Jové, J. A. K. Howard and P. J. Low, *J. Am. Chem. Soc*., 2008, **130**, 3566; (b) B. S. Brunschwig, C. Creutz and N. Sutin, *Coord. Chem. Re*v., 1998, **177**, 61; (c) C. Lambert, C. Risko, V. Coropceanu, J. Shelter, S. Amthor, N. E.; Gruhn, J. C. Durivage and J. L. Brédas, *J. Am. Chem. Soc*., 2005, **127**, 8508; (d) J.-P. Launay, *Chem. Soc. Re*v., 2001, **30**, 386.

2 (a) R. L. Carroll and C. B. Gorman, *Angew. Chem. Int. Ed*., 2002, **41**, 4378; (b) A. C. Benniston, *Chem. Soc. Re*v., 2004, **33**, 573; (c) P. J. Low, *Dalton Trans*., 2005, 2821. (d) T. Ren, *Organometallics*, 2005, **24**, 4854; (e) F. Paul and C. Lapinte, *Coord. Chem. Rev*., 1998, **178-180**, 431; (f) R. E. Martin and F. Diederich, *Angew. Chem*., 1999, **111**, 1440; (g) R. E. Martin and F. Diederich, *Angew. Chem. Int. Ed*., 1999, **38**, 1350; (h) C.-J. Yao, Y.-W. Zhong and J. N. Yao, *J. Am. Chem. Soc*., 2011, **133**, 15697; (i) J. Maurer , B. Sarkar, B. Schwederski, W. Kaim, R. F. Winter and S. Záliš, *Organometallics*, 2006, **25**, 3701; (j) F. Pevny, E. Di Piazza, L. Norel, M. Drescher, R. F. Winter and S. Rigaut, *Organometallics*, 2010, **29**, 5912.

3 (a) I. R. Whittall, A. M. McDonagh, M. G. Humphrey and M. Samoc, *Adv. Organomet. Chem*., 1998, **43**, 349; (b) M. Mayor, C. von Hänisch, H. B. Weber, J. Reichert and D. Beckmann, *Angew. Chem*., 2002, **114**, 1228; (c) M. Mayor, C. von Hänisch, H. B. Weber, J. Reichert and D. Beckmann, *Angew. Chem. Int. Ed*., 2002, **41**, 1183; (d) T. L. Schull, J. G. Kushmerick, C. H. Patterson, C. George, M. H. Moore, S. K. Pollack and R. Shashidhar, *J. Am. Chem. Soc*., 2003, **125**, 3202; (e) P. Aguirre-Etcheverry and D. O'Hare, *Chem. Rev*., 2010, **110**, 4839; (f) J. Maurer, M. Linseis, B. Sarkar, B. Schwederski, M. Niemeyer, W. Kaim, S. Záliš, C. Anson, M. Zabel and R. F. Winter, *J. Am. Chem. Soc*., 2008, **130**, 259; (g) M. Linseis, S. Záliš, M. Zabel and R. F. Winter, *J. Am. Chem. Soc*., 2012, **134**, 16671; (h) S. Záliš, R. F. Winter and W. Kaim, *Coord. Chem. Rev*., 2010, **254**, 1383; (i) V. Lloveras, A. Caballero, A. Tárraga, M. D. Velasco, A. Espinosa, K. Wurst, D. J. Evans, J. Vidal-Gancedo, C. Rovira, P. Molina and J. Veciana, *Eur. J. Inorg. Chem*., 2005, 2436.

4 (a) T. Ren, G. Zou and J. C. Alvarez, *Chem. Commun*., 2000, 1197; (b) H. M. Y. Ahmed, N. Coburn, D. Dini, J. J. D. de Jong, C. Villani, W. R. Browne and J. G. Vos. *Inorg. Chem*., 2011, **50**, 5861; (c) T. Ren and G. L. Xu, *Comments Inorg. Chem*., 2002, **23**, 355; (d) G.-L. Xu, G. Zou, Y.-H. Ni, M. C. DeRosa, R. J. Crutchley and T. Ren, *J. Am. Chem. Soc*., 2003, **125**, 10057; (e) G.-L. Xu, M. C. DeRosa, R. J. Crutchley and T. Ren, *J. Am. Chem. Soc*., 2004, **126**, 3728; (f) Y. H. Shi, G. T. Yee, G. B. Wang and T. Ren, *J. Am. Chem. Soc*., 2004, **126**, 10552; (g) G.-L. Xu, R. J. Crutchley, M. C. DeRosa, Q.-J. Pan, H. -X. Zhang, X. Wang and T. Ren, *J. Am. Chem. Soc*., 2005, **127**, 13354; (h) A. S. Blum, T. Ren, D. A. Parish, S. A. Trammell, M. H. Moore, J. G. Kushmerick, G.-L. Xu, J. R. Deschamps, S. K. Pollack and R. Shashidhar, *J. Am. Chem. Soc*., 2005, **127**, 10010; (i) T. Ren, *Organometallics*, 2005, **24**, 4854; (j) B. Xi, G.-L. Xu, P. E. Fanwick and T. Ren, *Organometallics*, 2009, **28**, 2338.

5 (a) S. Rigaut, J. Massue, D. Touchard, J.-L. Fillaut, S. Golhen and P. H. Dixneuf, *Angew. Chem. Int. Ed*., 2002, **41**, 4513; (b) S. Rigaut, C. Olivier, K. Costuas, S. Choua, O. Fadhel, J. Massue, P. Turek, J.-Y. Saillard, P. H. Dixneuf and D. Touchard, *J. Am. Chem. Soc*., 2006, **128**, 5859; (c) C. Olivier, S. Choua, P. Turek, D. Touchard and S. Rigaut, *Chem. Commun*., 2007, **128**, 3100; (d) N. Gauthier, C. Olivier, S. Rigaut, D. Touchard, T. Roisnel, M. G. Humphrey and F. Paul, *Organometallics*, 2008, **27**, 1063.

6 L.-B. Gao, S.-H. Liu, L.-Y. Zhang, L.-X. Shi and Z.-N. Chen, *Organometallics*, 2006, **25**, 506.

7 (a) S. H. Liu, Y. Chen, K. L. Wan, T. B. Wen, Z. Zhou, M. F. Lo, I. D. Williams and G. Jia, *Organometallics*, 2002, **21**, 4984; (b) S. H. Liu, H. P. Xia, T. B. Wen, Z. Y. Zhou and G. Jia, *Organometallics*, 2003, **22**, 737; (c) P. Yuan, S. H. Liu, W. Xiong, J. Yin, G. Yu, H. Y. Sung, I. D. Williams and G. Jia, *Organometallics*, 2005, **24**, 3966; (d) S. H. Liu, Q. Y.Hu, P. Xue, T. B. Wen, I. D. Williams and G. Jia, *Organometallics*, 2005, **24**, 769; (e) P. Yuan, X. H. Wu, G. Yu, D. Du and S. H. Liu, *J. Organomet. Chem*., 2007, **692**, 3588; (f) P. Yuan, J. Yin, G. Yu, Q. Y. Hu and S. H. Liu, *Organometallics*, 2007, **26**, 196; (g) S. H. Liu, H. Xia, K. L. Wan, R. C. Y. Yeung, Q.

Y. Hu and G. Jia, *J. Organomet. Chem*., 2003, **683**, 331; (h) H. P. Xia, R. C. Y. Yeung and G. Jia, *Organometallics*, 1998, **17**, 4762; (i) X. X. Zhu, Y. P. Ou, J. Zhang, J.-L. Xia, J. Yin, G.-A. Yu and S.-H. Liu, *Dalton Trans*., 2013, **42**, 7177.

8 (a) K. A. Green, M. P. Cifuentes, T. Christopher Corkery, M. Samoc and M. G. Humphrey, *Angew. Chem. Int. Ed*., 2009, **48**, 7867. (b) Y.-W. Zhong, N. Vila, J. C. Henderson, S. Flores-Torres and H. D. Abruña, *Inorg. Chem*., 2007, **46**, 10470.

9 (a) Y. Tanaka, T. Ishisaka, A. Inagaki, T. Koike, C. Lapinte and M. Akita, *Chem. Eur. J*., 2010, **16**, 4762; (b)Y. Tanaka, A. Inagaki and M. Akita, *Chem. Commun*., 2007, 1169; (c) K. Uchida, A. Inagaki and M. Akita, *Organometallics*, 2007, **26**, 5030. (d) K. Motoyama, T. Koike and M. Akita, *Chem. Commun*., 2008, 5812; (e) Y. Liu, C. Lagrost, K. Costuas, N. Tchouar, H. Le Bozec and S. Rigaut, *Chem. Commun*., 2008, 6117; (f) Y. Lin, J. Yuan, M. Hu, J. Cheng, J. Yin, S. Jin and S. H. Liu, *Organometallics*, 2009, **28**, 6402; (g) R.T. F. Jukes, V. Adamo, F. Hartl, P. Belser and L. De Cola, *Inorg. Chem*., 2004*,* **43**, 2779.

10 E. C. Harvey, B. L. Feringa, J. G. Vos, W. R. Browne and M. T. Pryce. *Coord. Chem. Rev*., 2015, **282-283**, 77.

11 (a) T. L. Stott and M. O. Wolf, *Coord. Chem. Rev*., 2003, **246**, 89; (b) J.-P. Launay, *Coord. Chem. Rev*., 2013, **257**, 1544.

12 L. G. Reuter, A. G. Bonn, A. C. St ckl, B. He, B. B. Pati, S. S. Zade and O. S. Wenger, *J. Phys. Chem. A*, 2012, **116**, 7345.

13 L.-B. Gao, J. Kan, Y. Fan, L.-Y. Zhang, S. H. Liu and Z.-N. Chen, *Inorg. Chem*., 2007, **46**, 5651.

14 (a) J. Bonvoisin, J.-P. Launay, M. van der Auweraer and F. C. de Schryver, *J. Phys. Chem.*, 1994, **98**, 5052; (b) J. Bonvoisin, J. P. Launay, W. Verbouwe, M. van der Auweraer and F. C. de Schryver, *J. Phys. Chem.*, 1996, **100**, 17079; (c) J. Sedo, D. Ruiz, J. Vidal Gancedo, C. Rovira, J. Bonvoisin, J. P. Launay and J. Veciana, *Adv. Mater.*, 1996, **8**, 748.

15 (a) M. Uno and P. H. Dixneuf, Angew. *Chem. Int. Ed*., 1998, **37**, 1714; (b) N. Ohshiro, F. Takei, K. Onitsuka and S. Takahashi, *Chem. Lett*., 1996, 871; (c) T. Weyland, C. Lapinte, G. Frapper, M. J. Calhorda, J.-F. Halet and L. Toupet,

Organometallics, 1997, **16**, 2024; (d) H. Fink, N. J. Long, A. J. Martin, G. Opromolla, A. J. P. White, D. J. Williams and P. Zanello, *Organometallics*, 1997, **16**, 2646.

16 (a) T. Weyland, C. Lapinte, G. Frapper, M. J. Calhorda, J.-F. Halet and L. Toupet, *Organometallics*, 1997, **16**, 2024; (b) Tania. Weyland, K. Costuas, A. Mari, J.-F. Halet and C. Lapinte, *Organometallics*, 1998, **17**, 5569; (c) T. Weyland, K. Costuas, L. Toupet, J.-F. Halet and C. Lapinte. *Organometallics*, 2000, **19**, 4228; (d) U. Pfaff, A. Hildebrandt, D. Schaarschmidt, T. Hahn,; S. Liebing, J. Kortus, H. Lang, *Organometallics*, 2012, **31**, 6761; (e) A. K. Diallo, C. Absalon, J. Ruiz, D. Astruc, *J. Am. Chem. Soc*., 2011, **133**, 629.

17 (a) U. Pfaff, A. Hildebrandt, D. Schaarschmidt, T. Hahn, S. Liebing, J. Kortus and H. Lang, *Organometallics*, 2012, **31**, 6761; (b) J. M. Speck, R. Claus, A. Hildebrandt, T. Rüffer, E. Erasmus, L. van As, J. C. Swarts and H. Lang, *Organometallics*, 2012, **31**, 6373; (c) M. Linseis, R. F. Winter, B. Sarkar, W. Kaim and S. Záliš, *Organometallics*, 2008, **27**, 3321; (d) A. Hildebrandt and H. Lang, *Organometallics*, 2013, **32**, 5640; (e) A. Hildebrandt, T. Rüffer, E. Erasmus, J. C. Swarts and H. Lang, *Organometallics*, 2010, **29**, 4900; (f) J. M. Speck, D. Schaarschmidt and H. Lang, *Organometallics*, 2012, **31**, 1975.

18 (a) X. C. Li and H. Tian, *Tetrahedron Lett*., 2005, **46**, 5409; (b) M. Irie, T. Fukaminato, K. Matsuda and S. Kobatake. *Chem. Rev*., 2014, **114**, 12174; (c) M. Irie, *Chem. Rev*., 2000, **100**, 1685; (c) M. Irie and M. Mohri, *J. Org. Chem*., 1988, **53**, 803.

19 K. C. Kemp, E. Fourie, E. J. Conradie and J. C. Swarts, *Organometallics*, 2008, **27**, 353.

20 W. R. Goetsch, P. V. Solntsev, C. van Stappen, A. A. Purchel, S. V. Dudkin and V. N. Nemykin. *Organometallics*, 2014, **33**, 145.

21 F. Barrière and W. E. Geiger, *J. Am. Chem. Soc*., 2006, **128**, 3980.

22 (a) S. Trupia, A. Nafady and W. E. Geiger, *Inorg. Chem*., 2003, **42**, 5480; (b) W. E. Geiger and F. Barrière, *Acc. Chem. Res*., 2010, **43**, 1030; (c) F. Barrière, N. Camire, W. E. Geiger, U. T. Mueller-Westerhoff and R. Sanders, *J. Am. Chem. Soc*., 2002, **124**, 7262; (d) D. Miesel, A. Hildebrandt, M. Korb, D. A. Wild, P. J. Low and H. Lang, *Chem. Eur. J*., 2015, **21**, 1545.

23 (a) N. Gauthier, N. Tchouar, F. Justaud, G. Argouarch, M. P. Cifuentes, L. Toupet, D. Touchard, J.-F. Halet, S. Rigaut, M. G. Humphrey, K. Costuas and F. Paul. *Organometallics*, 2009, **28**, 2253; (b) E. Wuttke, F. Pevny, Y.-M. Hervault, L. Norel, M. Drescher, R. F. Winter and S. Rigaut. *Inorg. Chem*., 2012, **51**, 1902; (c) K. Costuas, O. Cador, F. Justaud, S. Le Stang, F. Paul, A. Monari, S. Evangelisti, L. Toupet, C. Lapinte and J.-F. Halet. *Inorg. Chem*., 2011, **50**, 12601; (d) D.-B. Zhang, J.-Y. Wang, H.-M. Wen and Z.-N. Chen. *Organometallics*, 2014, **33**, 4738; (e) C.-J. Yao, H.-J. Nie, W.-W. Yang, J. Yao and Y.-W. Zhong. *Inorg. Chem*., 2015, **54**, 4688.

24 J. Beck, T. Bredow and R. T. Z. Triandi Tjahjanto, *Naturforsch*. 2009, **64b**, 145.

25 N. S. Rizalman, C. Capel Ferrón, W. Niu, A. L. Wallace, M. He, R. Balster, J. Lampkin, V. Hernández, J. T. López Navarrete, M. C. Ruiz Delgado and F. Hartl. *RSC Adv*., 2013, **3**, 25644.

26 (a) P. Mücke, M. Linseis, S. Záliš and R. F. Winter, *Inorg. Chim. Acta*, 2011, **374**, 36; (b) J. Maurer, B. Sarkar, W. Kaim, R. F. Winter and S. Záliš, *Chem. Eur. J*., 2007, **13**, 10257.

27 (a) M. Parthey, J. B. G. Gluyas, M. A. Fox, P. J. Low and M. Kaupp, *Chem. Eur. J*., 2014, **20**, 6895; (b) S. Marqués-González, M. Parthey, D. S. Yufit, J. A. K. Howard, M. Kaupp and P. J. Low, *Organometallics*, 2014, **33**, 4947; (c) M. Parthey, J. B. G. Gluyas, P. A. Schauer, D. S. Yufit, J. A. K. Howard, M. Kaupp and P. J. Low, *Chem. Eur. J*., 2013, **19**, 9780; (d) M. Parthey and M. Kaupp, *Chem. Soc. Rev*., 2014, **43**, 5067.

28 Y.-P. Ou, J. Xia, J. Zhang, M. Xu, J. Yin, G.-A. Yu and S. H. Liu, *Chem. Asian J*., 2013, **8**, 2023.

29 E. Wuttke, Y.-M. Hervault, W. Polit, M. Linseis, P. Erler, S. Rigaut and R. F. Winter. *Organometallics*, 2014, **33**, 4672.

30 (a) K. Costuas, O. Cador, F. Justaud, S. Le Stang, F. Paul, A. Monari, S. Evangelisti, L. Toupet, C. Lapinte and J.-F. Halet, *Inorg. Chem*., 2011, **50**, 12601; (b) E. C. Fitzgerald, A. Ladjarafi, N. J. Brown, D. Collison, K. Costuas, R. Edge, J.-F. Halet, F. Justaud, P. J. Low, H. Meghezzi, T. Roisnel, M. W. Whiteley and C. Lapinte, *Organometallics*, 2011, **30**, 4180.

31 (a) S. D. Glovera, J. C. Goeltza, B. J. Learb, C. P. Kubiak. *Coord. Chem. Re*v., 2010, **254**, 331; (b) J. B. G. Gluyas, A. J. Boden, S. G. Eaves, H. Yua and P. J. Low, *Dalton Trans*., 2014, **43**, 6291; (c) Z.-L. Gong, Y.-W. Zhong and J. N. Yao. *Chem. Eur. J.*, 2015, **21**, 1554; (d) D. J. Armitt, M. I. Bruce, M. Gaudio, N. N. Zaitseva, B. W. Skelton, A. H. White, B. Le Guennic, J.-F. Halet, M. A. Fox, R. L. Roberts, F. Hartl and P. J. Low. *Dalton Trans*., 2008, 6763; (e) H.-J. Nie, C.-J. Yao, J.-Y. Shao, J. N. Yao and Y.-W. Zhong. *Chem. Eur. J.*, 2014, **20**, 17454; K. Tahara, T. Akita, S. Katao and J. Kikuchi, *Dalton Trans*., 2014, **43**, 1368.

32 (a) A. Burgun, F. Gendron, C. Sumby, T. Roisnel, O. Cador, K. Costuas, J.-F. Halet, M. I. Bruce and C. Lapinte, *Organometallics*, 2014, **33**, 2613; (b) R. Makhoul, Y. Kumamoto, A. Miyazaki, F. Justaud, F. Gendron, J.-F. Halet, J.-R. Hamon and C. Lapinte, *Eur. J. Inorg. Chem*., 2014, 3899; (c) R. Makhoul, H. Sahnoune, V. Dorcet, J.-F. Halet, J.-R. Hamon and C. Lapinte, *Organometallics*, 2015, **34**, 3314; (d) J. Zhang, M.-X. Zhang, C.-F. Sun, M. Xu, F. Hartl, J. Yin, G.-A. Yu, L. Rao and S.-H. Liu, *Organometallics*, 2015, **34**, 3967.

33 X. Li, B. Wang, Y.-A. Son, J. Wang and S. Wang, *Z. Kristallogr. NCS*, 2009, **224**, 697.

34 X. Li, B. Wang, Y.-A. Son, J. Wang and S. Wang, *Z. Kristallogr. NCS*, 2009, **224**, 691.

35 E. Kozma, F. Munno, D. Kotowski, F. Bertini, S. Luzzati and M. Catellani, *Synth. Met*., 2010, **160**, 996.

36 D. R. Coulson, *Inorg. Synth*., 1990, **28**, 121.

37 N. Ahmad, J. J. Levison, S. D. Robinson, M. F. Uttley, E. R. Wonchoba and G. W. Parshall, *Inorg. Synth*., 1974, **15**, 45.

38 F. Poul, B. G. Eillis, M. I. Bruce, L. Toupet, T. Costuas, J.-F. Halet and C. Lapinte, *Organometallics*, 2006, **25**, 649.

39 M. Krejčík, M. Daněk and F. Hart1, *J. Electroanal. Chem. Interfacial Electrochem*., 1991, **317**, 179.

40 Gaussian 09, Revision D.01, M. J. Frisch, G. W. Trucks, H. B. Schlegel, G. E. Scuseria, M. A. Robb, J. R. Cheeseman, G. Scalmani, V. Barone, B. Mennucci, G. A.

Petersson, H. Nakatsuji, M. Caricato, X. Li, H. P. Hratchian, A. F. Izmaylov, J. Bloino, G. Zheng, J. L. Sonnenberg, M. Hada, M. Ehara, K. Toyota, R. Fukuda, J. Hasegawa, M. Ishida, T. Nakajima, Y. Honda, O. Kitao, H. Nakai, T. Vreven, J. A. Montgomery, Jr., J. E. Peralta, F. Ogliaro, M. Bearpark, J. J. Heyd, E. Brothers, K. N. Kudin, V. N. Staroverov, R. Kobayashi, J. Normand, K. Raghavachari, A. Rendell, J. C. Burant, S. S. Iyengar, J. Tomasi, M. Cossi, N. Rega, J. M. Millam, M. Klene, J. E. Knox, J. B. Cross, V. Bakken, C. Adamo, J. Jaramillo, R. Gomperts, R. E. Stratmann, O. Yazyev, A. J. Austin, R. Cammi, C. Pomelli, J. W. Ochterski, R. L. Martin, K. Morokuma, V. G. Zakrzewski, G. A. Voth, P. Salvador, J. J. Dannenberg, S. Dapprich, A. D. Daniels, Ö. Farkas, J. B. Foresman, J. V. Ortiz, J. Cioslowski, and D. J. Fox, Gaussian, Inc., Wallingford CT, 2009.

41 M. Renz, K. Theilacker, C. Lambert and M. Kaupp, *J. Am. Chem. Soc*., 2009, **131**, 16292.

42 (a) V. Barone and M. Cossi, *J. Phys. Chem. A*, 1998, **102**, 1995; (b) M. Cossi, N. Rega, G. Scalmani and V. Barone, *J. Comput. Chem*., 2003, **24**, 669.

43 A. P. Scott and L. Radom, *J. Phys. Chem*., 1996, **100**, 16502.

44 J. C. Röder, F. Meyer, I. Hyla-Kryspin, R. F. Winter and E. Kaifer, *Chem. Eur. J.* 2003, **9**, 2636.

A series of di- and trinuclear ruthenium vinyl and ethynyl oligothiophene complexes have been synthesized and characterised. Their anodic behavior was investigated by spectro-electrochemical methods. The experimental results and DFT calculations have consistently revealed that the open triruthenium complexes exhibit stepwise laterally localized oxidation processes.

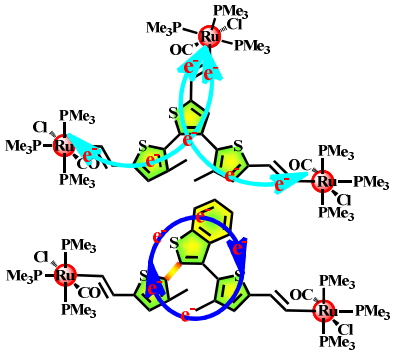

Jing Zhang, Chao-Fang Sun, Ming-Xing Zhang, František Hartl, Jun Yin, Guang-Ao Yu, Li Rao, Sheng Hua Liu**

Page No. – Page No.

Asymmetric oxidation of bridging vinyl- and ethynyl terthiophene ligands in trinuclear ruthenium complexes